

Master of Science in Computational Mechanics

Universitat Politècnica de Catalunya

Three dimensional modelling of fibre reinforced
composite materials for aerospace applications

By

Shankara Narayana Phaneendra

June 2009

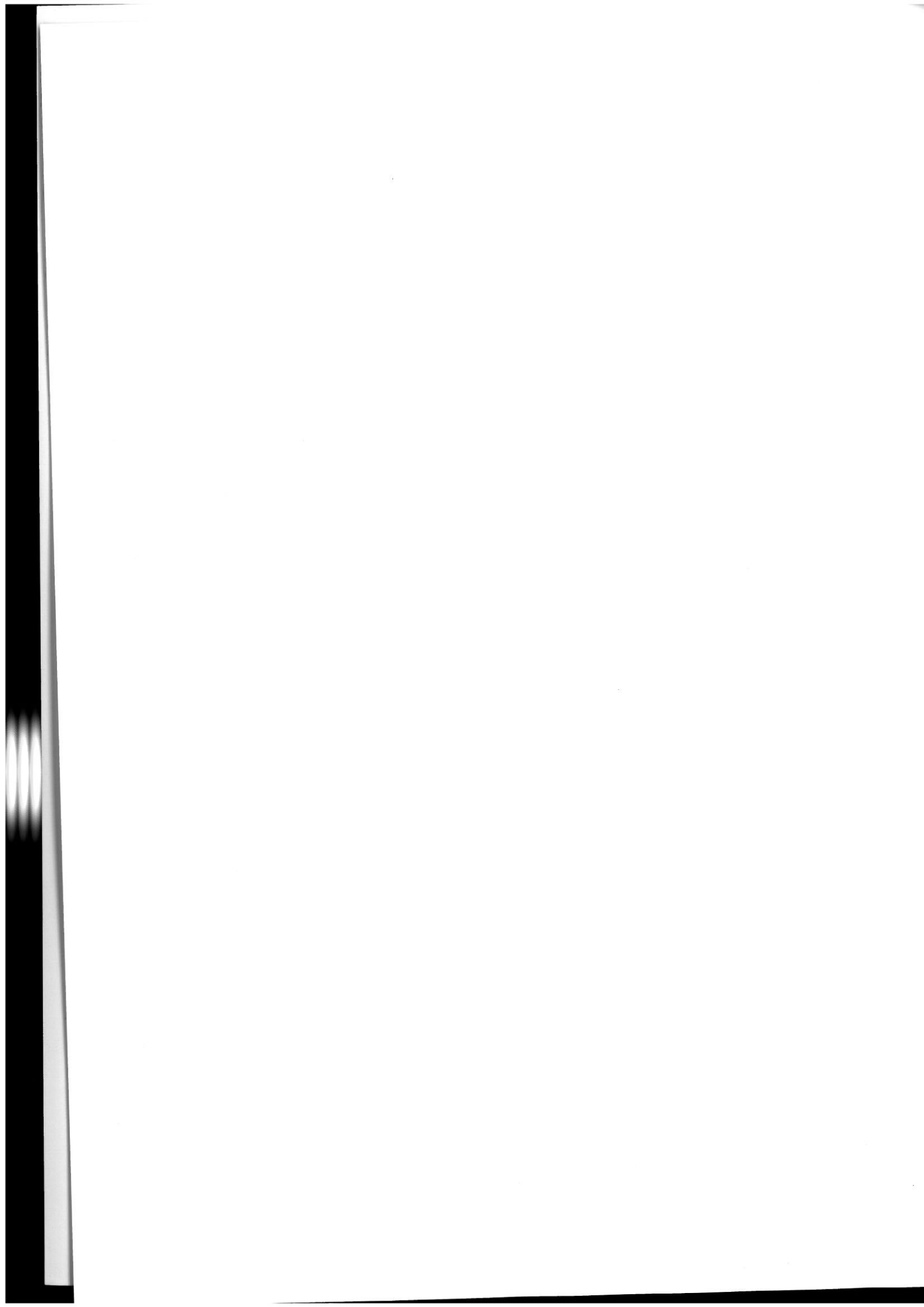
This thesis is submitted in partial fulfillment of the requirements for the Degree
of MSc in Computational Mechanics

Master's Thesis

Advisors: Dr. J.L. Curiel Sosa

&

Prof. Antonio Rodriguez-Ferran



ABSTRACT

Composites are fast replacing the conventional materials especially in the aircraft industry due to their high stiffness to weight and high strength to weight ratios. Aircraft structures are subjected to various hazards during their service. One of the most dangerous hazards is that of the bird strike on structures during flight. The fan blades of the compressor of the jet engine are prone to such hazards. With this being the case, it becomes very important to study the failure phenomenon in composites. As, the experimental approach to study the failure phenomenon turns out to be very costly, the only recourse is to computer simulations. This necessitates the need for appropriate mathematical modeling of the composite material structures subjected to high velocity impact.

This thesis describes the work carried out to implement a three dimensional mixed mode damage model for composites subjected to high velocity impact. The model considers the four intralaminar failure modes: fiber rupture, fiber buckling, matrix cracking and matrix crushing. The model considers a non-linear gradual degradation of the stiffness after the initiation of failure.

The model has been implemented in the Abaqus subroutine VUMAT. The tension and compression tests for a single element along the three mutually perpendicular directions have been conducted and stress-strain curves plotted. The stress-strain curves for a single element for tension and compression tests are found to be satisfactory. A low velocity impact simulation has been carried out to further assess the capability of the model.

Future work along these lines would be to include explicitly another widely observed failure mode, that is delamination into the model and also to account for the non-linear shear stress-strain behavior. Also, calibration of the directional damage vectors could be done in order to yield better results.

Acknowledgements

The author would like to thank Dr. J.L. Curiel Sosa for providing an opportunity to work on this topic that has brought enormous joy and pleasure along with a good learning experience. The author thanks the same for his constant support and guidance throughout the thesis work. The author is grateful to Dr. J.L. Curiel Sosa for providing guidance in carrying out internship work at Rolls-Royce Plc. The author is grateful to the same for the patience he demonstrated while providing corrections and suggestions for the thesis write up. The author would like to thank Dr. J.L. Curiel Sosa for his concern during the author's ill-health. The author would like to appreciate the career guidance provided by the same.

The author would also like to thank Prof. Antonio Rodriguez-Ferran for his constant support and guidance with regard to the thesis write up and the thesis presentation.

The author would also like to thank the faculties of LACAN and CIMNE for providing excellent course work.

The author is grateful to the staff of Rolls- Royce Plc for their co-operation and support during the internship.

The author would like to recognize the kind attention and administrative support provided by Lelia Zielonka (CIMNE).

The author would also like to thank his parents (Anna, Amma) and other family members (Kumarji, Chikkamma, Jiju, Manu, Satisha and Chinnu) for their encouragement and solidarity all throughout the Master's degree.

Contents

Abstract.....	iii
Acknowledgements.....	iv
Contents.....	v
List of Figures.....	viii
List of Tables.....	xi
1. Introduction.....	1
1.1. Motivation.....	1
1.2. Thesis objective.....	3
1.3. Outline.....	4
2. Literature survey.....	5
2.1. Brief state of art.....	5
2.2. Detailed Review.....	6
2.2.1. Strength based stress or strain criteria to predict failure.....	6
2.2.2. Interactive stress based criteria to predict failure.....	7
2.2.3. Two dimensional progressive damage model.....	9
2.2.4. Three dimensional progressive damage model.....	10
2.2.5. Progressive failure analysis.....	12
2.3. Conclusions.....	13
3. Damage prediction with the state of art failure theories.....	14
3.1 Introduction.....	14
3.2. A brief about the software.....	15
3.2.1. Material parameter calculation.....	15
3.2.2. A brief about the failure criteria employed by the software.....	16
3.2.3. Failure prediction.....	18
3.3. Description of the analysis carried out.....	20
3.3.1. Description of the specimen.....	20

3.3.2. Material Parameters and the stacking sequence.....	22
3.4. Results.....	23
3.4.1. Plot of force displacement curve.....	26
3.5 Conclusions.....	27
4. Implementation of the Damage Model.....	28
4.1. Introduction.....	28
4.2. Assumptions.....	28
4.3. The description of the model.....	29
4.3.1 Evolution of damage.....	31
4.4. Formulation implemented in Abaqus VUMAT.....	32
4.5. Tension Test along the fiber direction with one element with one gauss point.....	33
4.5.1. Results for the tension test.....	35
4.6. Compression test along the fiber direction on a cube with one element with one gauss point.....	37
4.6.1. Results for the compression test.....	37
4.7. Tension test along the first transverse direction on a cube with one element with one gauss point.....	39
4.7.1. Results for the Tension test.....	39
4.8. Compression test along the first transverse direction on a cube with one element with one gauss point.....	40
4.8.1. Results for the compression test.....	40
4.9. Tension test along the second transverse direction on a cube with one element with one gauss point.....	42
4.9.1. Results for the Tension test.....	42
4.10. Compression test along the second transverse direction on a cube with one element with one gauss point.....	43
4.10.1. Results for the Tension test.....	43
4.11. Shear Stress-Strain relationship in 12 Plane.....	45
4.12. Shear Stress-Strain relationship in 13 Plane.....	46
4.13. Shear Stress-Strain relationship in 23 Plane.....	47
4.14. Modes of damage observed.....	48
4.15. Low velocity impact analysis on composite target.....	50

4.15.1. Experimental test and results	50
4.15.2. Numerical simulation using mixed mode damage model.....	52
4.15.3. Discussion of results	56
5. Conclusions and Further Work	58
5.1. Conclusions	58
5.2. Future Work	60
References	61

List of Figures

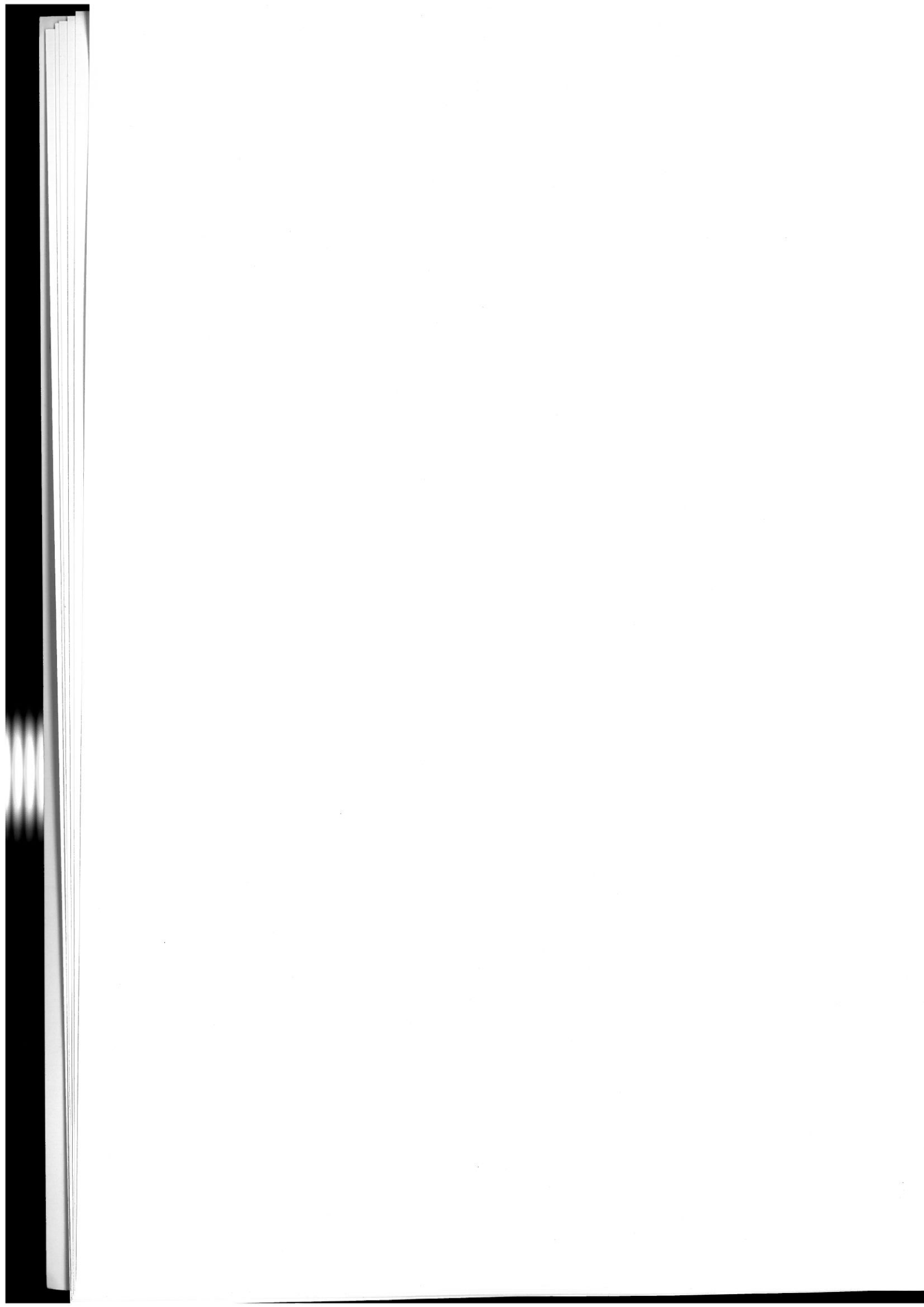
Figure 1.1.Increased use of composite material in newer versions of F-18 Hornet.	1
Figure 1.2.Dangerous bird strike events.	2
Figure 1.3.Matrix cracking.	3
Figure 1.4.Fiber kinking.	3
Figure 1.5.Fiber rupture.	3
Figure 1.6.Delamination.	3
Figure 3.1.Fan blade and jet engine.	14
Figure 3.2.Scheme adopted to calculate the properties.	15
Figure 3.3.Test to caculate strength properties.	16
Figure 3.4.Progression of failure from lamina to structure.	20
Figure 3.5.Complete Model.	20
Figure 3.6.1/8 th Model	21
Figure 3.7.Boundary Conditions specified for the specimen	21
Figure 3.8.Damage pattern predicted by MDE	23
Figure 3.9.Damage pattern predicted by Puck	24
Figure 3.10.Damage pattern predicted by Tsai-Hill	25
Figure 3.11.Damage pattern predicted by Tsai-Wu	25
Figure 3.12.Comparison of the force dispalcement diagrams for various criteria	26
Figure 4.1.Boundary conditions specified on the cube	35
Figure 4.2.Stress distribution in the cube	35
Figure 4.3.Displacement in the cube	36
Figure 4.4.Stress strain curve for the cube for tension along the fiber	36

Figure 4.5. Variation of phi over time for fiber rupture	37
Figure 4.6. Stress strain curve for the cube for compression along the fiber	38
Figure 4.7. Variation of phi over time for fiber buckling	38
Figure 4.8. Stress strain curve for the cube for tension along the first transverse fiber	39
Figure 4.9. Variation of phi over time for matrix cracking along the first transverse fiber	40
Figure 4.10. Stress strain curve for the cube for compression along the first transverse direction..	41
Figure 4.11. Variation of phi over time for matrix crushing along the first transverse direction	41
Figure 4.12. Stress strain curve for the cube for tension along the second transverse direction	42
Figure 4.13. Variation of phi over time for matrix cracking along the second transverse direction	43
Figure 4.14. Stress strain curve for the cube for compression along the second transverse direction.....	44
Figure 4.15. Variation of phi over time for matrix crushing along the second transverse direction	44
Figure 4.16. Stress strain curve for the cube in the 1-2 plane	45
Figure 4.17. Stress strain curve for the cube in the 1-3 plane	46
Figure 4.18. Stress strain curve for the cube in the 2-3 plane	47
Figure 4.19. Experimental setup for the low velocity impact test.....	50
Figure 4.20. Experimental setup for the target and the support	51
Figure 4.21. Delamination pattern observed in target plate with dye penetrant.....	51
Figure 4.22. Meshed geometry of the low velocity impact analysis	52
Figure 4.23. Boundary conditions specified on the target.....	54
Figure 4.24. Von mises stress distribution on the target.....	54
Figure 4.25. Distribution of stress component S33 on the target	55

Figure 4.26. Damage in the normal direction.....56

List of Tables

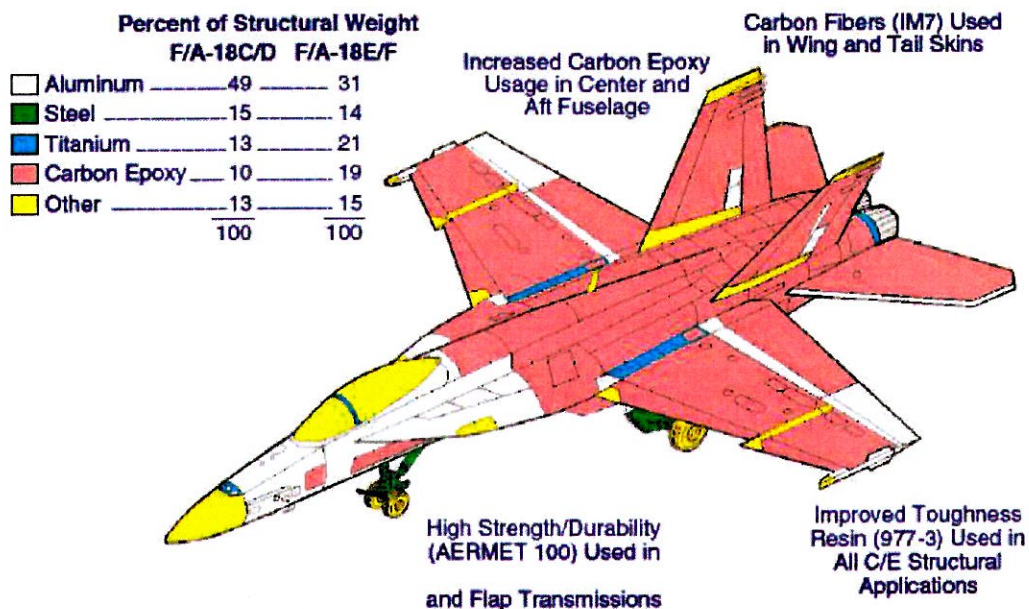
Table 3.1. List of strength based criteria with its description.	17
Table 3.2. List of properties of the specimen.	22
Table 4.1. List of properties of the composite laminate	34
Table 4.2. Table listing the properties of the impactor and the support	52
Table 4.3. Table listing the properties specified for the composite laminate	53



1. Introduction

1.1. Motivation

Composite materials are ideal for structural applications where high strength to weight and stiffness to weight ratios are required. With the enhancements in composite technology over the past years more and more aircrafts have a significant proportion of their structure made up of composite materials. Majority of composite aircraft structures are made up of Fiber reinforced plastics. They have properties that are similar to some other composites such as higher strength and stiffness when compared to aluminum alloys and also have an added advantage of being lighter in weight. Fiber reinforced plastics do however have some disadvantages such as their brittleness which means there is no plastic yielding and reduced strength due to impact damage which is sometimes not visible to the naked eye.



(Figure 1.1. Increased use of composite material in newer versions of F-18 Hornet. After "<http://images.google.es>")

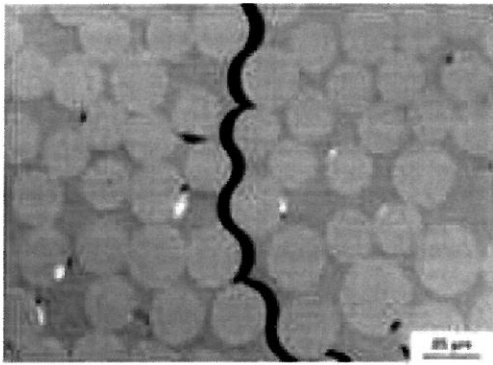
Until the introduction of the Boeing F/A-18E/F super hornet which has about 20% of its structure made of composite materials, the amount of composites used in its earlier version F/A-

18C/D was limited to only about 10% of the total structure as shown in the figure (1.1). This increasing trend seems only likely to continue in the future and therefore this places a strong need to investigate the response of composite materials to the type of dangers that an aircraft may experience during its lifetime. One of these dangers is bird strikes on critical aircraft components such as compressor fan blades, wing leading edges, windscreens as shown in the figure (1.2) etc.

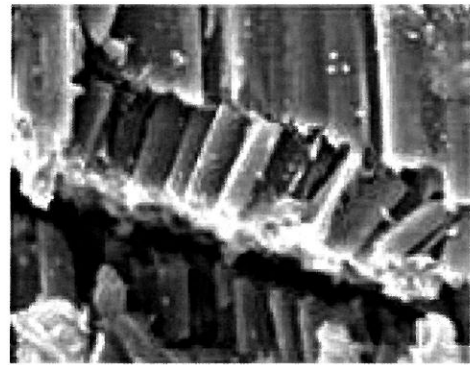


(Figure 1.2 – Dangerous bird strike events. After “<http://images.google.es>”)

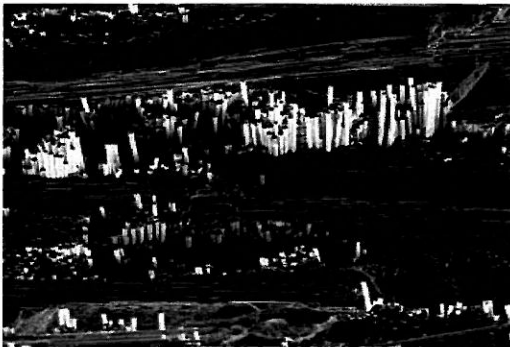
This is of major significance as this type of impact can lead to following damage modes in composite materials: matrix cracking as shown in figure (1.3), fiber failures i.e., fiber kinking as shown in figure (1.4), fiber rupture as shown in figure (1.5) and delamination as shown in figure (1.6). These failure modes can seriously weaken the composite material. The main techniques used to investigate the response of composite structures to impact are experimental and computational tests. For investigations on bird strike on composite structures experimental techniques can be expensive and time consuming while computational methods, although cheaper, difficulties arise in modeling the composite materials behavior due to impact loading. In order to simulate the response of composite structures due to bird impact it is important to use constitutive models capable of estimating their stiffness and strength.



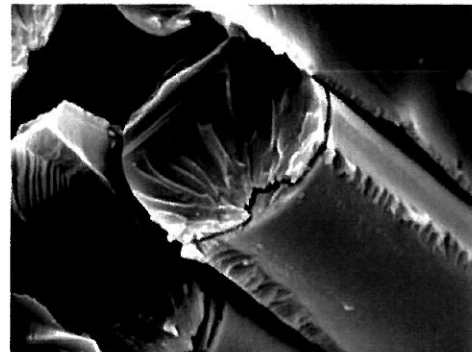
(Figure 1.3 – Matrix cracking.
After “www . compositeworld.com”)



(Figure 1.4 – Fiber Kinking.
After “www . compositeworld.com”)



(Figure 1.5 – Fiber rupture.
After “www . compositeworld.com”)



(Figure 1.6 – Delamination.
After “www . compositeworld.com”)

1.2. Thesis objective

The objective of the thesis is to implement the 3D mixed mode material model for the composite material structures subjected to high velocity impact, proposed by J.L.Curiel Sosa et al. [1]. The material model considers the following damage modes: fiber rupture, fiber kinking, matrix cracking and matrix crushing. The material model has been implemented in Abaqus subroutine VUMAT. The results have been satisfactory for single element tension and compression tests and shear tests. To continue further on these lines, it would be necessary to include delamination into the model and also model non linear the shear stress strain relationship.

1.3. Outline

The thesis is structured, beginning with a detailed review of the state of art of predicting failure in composite materials, followed by an investigation done to assess the capability of the state of failure theories. This followed by the formulation of the model and its implementation into Abaqus VUMAT subroutine. The results are presented for single element test. A description of a low velocity impact simulation conducted to further assess the capability of the model is presented, followed by concluding remarks and future work to be done on these lines.

2. Literature survey

2.1. Brief state of art

As far, the strategies for modeling failure in composite materials may be broadly classified into two approaches as pointed out by J.L.Curiel Sosa et al. [1]. The first approach assumes a linear elastic behavior followed by a complete loss of the stiffness. This approach makes use of strength based criteria such as maximum stress theory and maximum strain theory or interactive criteria such as Tsai-Hill and Tsai-Wu. A range of assessments of these criteria has been carried out in references [2, 3]. A considerable effort has been done in the search for a consensus amongst all these criteria that allows solving a range of problems. However, the exercises done by Soden et al. [4, 5] reveal discrepancies larger than 200 % as pointed out by Daniel [6].

Cuntze and Freund [7] state that for the assessment of the performance of a composite under failure, the conditions of damage onset are not as relevant as the prediction of stiffness degradation as its influence diminishes with the damage progression. This is in agreement with other theories that defend the inelastic behavior of the composite.

The second approach proposes a progressive evolution of the damage, although most of these last approaches are limited to two-dimensional models, generally assuming a plane stress state in the lamina, see for instance references [8-11]. References [12, 13] use state variables to describe the accumulation of damage which degrades the elastic properties.

However, a nonlinear regime was not considered in these first studies. Apparently, pioneering works on nonlinear mechanics of composites were developed in references [14, 15]. Both works are dedicated to the analysis of composite plates. A 2D nonlinear study devoted to the simulation of composite pinned-joint failure, proposed by Lessard and Shokrieh [16], points out those two-dimensional analyses generate sensibly different results as a consequence of the anisotropy induced by mixed-modes damage in the initially orthotropic composite.

More recently, Camanho et al. [17, 18] proposes a damage progression model operating jointly with interface elements to couple the damage evolution to the mechanics of the fracture. Zhodi et al. [19] presented an iterative algorithm for simulation of damage in composites through the reduction of the material stiffness at locations where a selection of constraints were infringed.

2.2. Detailed Review

In recent years, considerable attention has been focused on the modeling of composite materials as conventional materials are continuously being replaced by a variety of composite materials. Several approaches have been developed but there is still a strong need of predicting models that can be used for stiffness and strength assessment of this type of materials in actual situations without the need of many empirical constants.

There are various approaches adopted in the modeling of composite. One common approach is the use of the classical strength based criteria i.e., the stress based criteria or the strain based criteria. This approach assumes that the linear elastic behavior of the composite is followed by a sudden loss of the load bearing capacity. Most of these stress based criteria are mere extensions of the criteria for isotropic material.

The other approach is the use of the quadratic stress or strain based criteria, which are interactive criteria as there is interaction between the stresses in different directions. This accounts for the stresses developed in a direction other than the loading direction. This approach also assumes a linear elastic behavior of the composite followed by a sudden loss of the load bearing capacity.

The latest approach being progressive failure analysis of structure. In this approach a failure in the ply is propagated unto the failure of the structure. The failure of the ply is predicted by the use of interactive stress based and strength based criteria. There are no degradation models.

In this chapter, a detailed review of the various stress based criteria and the various other models and approaches is presented.

2.2.1. Strength based stress or strain criteria to predict failure

- Maximum stress theory

According to this theory, the tensile stresses in the principal material directions must be less than the respective strengths, otherwise fracture is said to have occurred [20].

$$\sigma_1 < X_t \quad (2.1)$$

$$\sigma_2 < Y_t \quad (2.2)$$

$$|\tau_{12}| < S \quad (2.3)$$

and for the compressive stresses

$$\sigma_1 > X_c \quad (2.4)$$

$$\sigma_2 > Y_c \quad (2.5)$$

The inequalities (2.1- 2.5) represent the maximum stress theory.

- Maximum strain theory

According to this theory, the tensile strains in the principal material directions must be less than the respective maximum strain limits, otherwise fracture is said to have occurred [20].

$$\epsilon_1 > X_{\epsilon t} \quad (2.6)$$

$$\epsilon_2 > Y_{\epsilon t} \quad (2.7)$$

$$|\gamma_{12}| > S_{\epsilon} \quad (2.8)$$

and for compressive strains

$$\epsilon_1 > X_{\epsilon c} \quad (2.9)$$

$$\epsilon_2 > Y_{\epsilon c} \quad (2.10)$$

The inequalities (2.6- 2.10) represent the maximum strain theory.

2.2.2. Interactive stress based criteria to predict failure

- Tsai-Hill Criteria

This criterion proposed as a yield criterion for composite materials can be used as strength criterion as the both being the limits of linear elastic behavior. This is an extension of the von Mises' isotropic yield criterion. This criterion can be represented by equation (2.11).

$$(G + H)\sigma_1^2 + (F + H)\sigma_2^2 + (F + G)\sigma_3^2 - 2H\sigma_1\sigma_2 - 2G\sigma_1\sigma_3 - 2F\sigma_2\sigma_3 + 2L\tau_{23}^2 + 2M\tau_{13}^2 + 2N\tau_{12}^2 = 1 \quad (2.10)$$

Where, F, G, H, L, M and N are related to the usual failure strengths X, Y and S. Using appropriate relations for the various parameters, the criterion finally can be written in terms of the X, Y and S as in equation (2.11).

$$\frac{\sigma_1^2}{X} - \frac{\sigma_1\sigma_2}{X} + \frac{\sigma_2^2}{Y} + \frac{\tau_{12}^2}{S} = 1 \quad (2.11)$$

This theory appears to be better than the maximum stress and maximum strain theory, as the agreement with the experimental work is good [20]. This considers interaction between the failure strengths X, Y and S.

- Tsai-Wu criteria

This criterion can be represented as in equation (2.12)

$$F = F_{ij} \sigma_i \sigma_j + F_i \sigma_i \quad (2.12)$$

Where $i, j = 1, 2, \dots, 6$ and summation conventions apply on repeated indices. The stresses are represented by the Voigt notation. The F_i and F_{ij} are strength tensors of the second and fourth rank respectively.

It is considered that if $F > 1$, the composite has failed. This theory is more general than the Tsai-Hill as it is invariant under rotation. Even though the determination of the term F_{12} is difficult; there is a good match between experimental results and the use of this theory [20].

- Puck's criterion

Fiber failure tension

$$\frac{1}{\varepsilon_{1T}} \left(\varepsilon_1 + \frac{v_{f12}}{E_{f1}} m_{\sigma f} \sigma_2 \right) = 1 \quad (2.13)$$

Inter-fiber failure mode A (for transverse tension)

$$\sqrt{\left(\frac{\tau_{21}}{S_{21}}\right)^2 + \left(1 - p_{\perp\parallel}^{(+)} \frac{Y_T}{S_{21}}\right)^2 \left(\frac{\sigma_2}{Y_T}\right)^2} + p_{\perp\parallel}^{(+)} \frac{\sigma_2}{S_{21}} = 1 - \frac{\sigma_1}{\sigma_{1D}} \quad (2.14)$$

Inter-fiber failure mode B (for moderate transverse compression)

$$\frac{1}{S_{21}} \left(\sqrt{\tau_{21}^2 + \left(p_{\perp\parallel}^{(-)} \sigma_2\right)^2} + p_{\perp\parallel}^{(-)} \sigma_2 \right) = 1 - \frac{\sigma_1}{\sigma_{1D}} \quad (2.15)$$

Inter-fiber failure mode C (for large transverse compression)

$$\left[\left(\frac{\tau_{21}}{2(1+p_{\perp\parallel}^{(-)})S_{21}} \right)^2 + \left(\frac{\sigma_2}{Y_c} \right)^2 \right] \frac{Y_c}{(-\sigma_2)} = 1 - \frac{\sigma_1}{\sigma_{1D}} \quad (2.16)$$

A detailed description about the model is available in the following reference [21].

2.2.3. Two dimensional progressive damage model

This model is also based on the continuum damage mechanics approach [22]. It considers the non linear inelastic behavior of the composite material after the initiation of damage; it assumes a plane stress condition. The failure criteria are represented as follows:

Tensile fiber mode

$$e_m^2 = \left(\frac{\sigma_{11}}{X_t} \right)^2 - 1 \quad (2.17)$$

Compressive fiber mode

$$e_m^2 = \left(\frac{\sigma_{11}}{X_c} \right)^2 - 1 \quad (2.18)$$

Tensile matrix mode

$$e_m^2 = \left(\frac{\sigma_{11}}{X_c} \right)^2 + \left(\frac{\tau}{S_c} \right)^2 - 1 \quad (2.19)$$

Compressive matrix mode

$$e_m^2 = \left(\frac{\sigma_{11}}{X_c} \right)^2 + \left(\frac{\tau}{S_c} \right)^2 - 1 \quad (2.20)$$

The compliance tensor is defined as in equation

$$H(\omega) = \begin{bmatrix} \frac{1}{(1-\omega_{11})E_{\parallel}} & -\frac{\nu_{21}}{E_{\parallel}} & 0 \\ -\frac{\nu_{21}}{E_{\parallel}} & \frac{1}{(1-\omega_{22})E_{\parallel}} & 0 \\ 0 & 0 & \frac{1}{(1-\omega_{12})G} \end{bmatrix} \quad (2.21)$$

The loading surfaces f_{\parallel} for the fiber damage modes and f_{\perp} for the matrix damage modes are defined as in equations (2.22-2.23).

$$f_{\parallel} = \frac{\sigma_{11}^2}{(1-\omega_{11c,t})^2 X_{c,t}^2} - r_{\parallel c,t} = 0 \quad (2.22)$$

$$f_{\perp} = \frac{\sigma_{22}^2}{(1-\omega_{22c,t})^2 Y_{c,t}^2} + \frac{r^2}{(1-\omega_{12})^2 S_c^2} - r_{\perp} = 0 \quad (2.23)$$

The evolution of damage variables is described as in equation (2.24).

$$\dot{\omega} = \sum_i \phi_i q_i \quad (2.24)$$

A detailed description of the model can be found in the reference [22].

2.2.4. Three dimensional progressive damage model

A damage model proposed by Camanho et al. [23] is a fully three dimensional continuum based damage model. The damage model assumes that the composite material is transversely isotropic and is implemented in an implicit finite element code. The model takes into account the failure mechanisms both at the intra laminar level and inter laminar level.

In this model, the complementary free energy is defined as in equation (2.17).

$$\Psi = \frac{\sigma_{11}^2}{2(1-d_1)E_1} + \frac{1}{2E_2} \left(\frac{\sigma_{22}^2}{1-d_2} + \frac{\sigma_{33}^2}{1-d_3} \right) - \frac{\nu_{12}}{E_1} (\sigma_{22} + \sigma_{33})\sigma_{11} - \frac{\nu_{23}}{E_2} \sigma_{22}\sigma_{33} + \frac{\sigma_{12}^2 + \sigma_{13}^2}{2(1-d_6)G_{12}} + [\alpha_{11}\sigma_{11} + \alpha_{22}(\sigma_{22} + \sigma_{33})] \Delta T +$$

$$[\beta_{11}\sigma_{11} + \beta_{22}(\sigma_{22} + \sigma_{33})] \Delta M \quad (2.25)$$

The damage variables d_1, d_2, d_3 in the longitudinal, first transverse direction and the second transverse direction are defines as in equations (2.18- 2.20) below.

$$d_1 = d_{L+} \frac{\langle \sigma_{11} \rangle}{|\sigma_{11}|} + d_{L-} \frac{\langle \sigma_{11} \rangle}{|\sigma_{11}|} \quad (2.26)$$

$$d_2 = d_{T+} \frac{\langle \sigma_{22} \rangle}{|\sigma_{22}|} + d_{T-} \frac{\langle \sigma_{22} \rangle}{|\sigma_{22}|} \quad (2.27)$$

$$d_3 = d_{T+} \frac{\langle \sigma_{33} \rangle}{|\sigma_{33}|} + d_{T-} \frac{\langle \sigma_{33} \rangle}{|\sigma_{33}|} \quad (2.28)$$

The damage activation functions are defined as in equations (2.21-2.23).

$$F_{L+} = \phi_{L+} - r_{L+} \leq 0 \quad (2.29)$$

$$F_{L-} = \phi_{L-} - r_{L-} \leq 0 \quad (2.30)$$

$$F_T = \phi_T - r_T \leq 0 \quad (2.31)$$

Where F_{L+} defines the elastic domain for longitudinal tensile failure, F_{L-} defines the elastic domain for the longitudinal compressive failure, and F_T defines the elastic domain for transverse failure.

The loading functions ϕ_N ($N = L+, L-, T$) depend on the strain tensor and on the elastic and strength properties. They are defined as in equations (2.28-2.30).

$$\phi_{L+} = \frac{E_1}{X_T} (\epsilon_{11}) \quad (2.32)$$

$$\phi_{L-} = \frac{E_1}{X_c} (-\epsilon_{11}) \quad (2.33)$$

$$\phi_T = \sqrt{\left(\frac{Y_c - Y_T}{Y_c Y_T}\right) (\sigma_{22} + \sigma_{33}) + \frac{1}{Y_c Y_T} (\sigma_{22} - \sigma_{33})^2 + \frac{\sigma_{12}^2 + \sigma_{13}^2}{S_L^2}} \quad (2.34)$$

The internal variable r_T is defined as in equation (2.31).

$$r_T = \max\{1, \max\{\phi_T^s\}\} \quad (2.35)$$

$$r_{L+} = \max\{1, \max\{\phi_{L+}^s\}, \max\{\phi_{L-}^s\}\} \quad (2.36)$$

$$r_{L-} = \max\{1, \max\{\phi_{L-}^s\}\} \quad (2.37)$$

For the damage evolution laws and a detailed description, please refer to the paper [23].

2.2.5. Progressive failure analysis

The other recently developed approach is the progressive failure analysis, which is implemented in one of popular commercial software. In this approach, the displacements, strains and stresses calculated at the node from the FEA solver are converted into lamina and laminate level using the classical laminate theory.

At the lamina level, the stresses calculated are verified against a set of failure criteria. Based on the failure criteria satisfied, the corresponding properties are reduced. For example, when the longitudinal strength criterion is satisfied, the young's modulus of both the matrix and the fiber is set to zero. Now, the stiffness and other properties of the structure are recalculated, taking into account the decreased stiffness of the lamina in the element.

As, damage accumulates in the element lamina by lamina, the stiffness of the element is set to zero, thereby reducing the load carrying capacity of the element to zero. When, this happens the element is deleted from the mesh.

This cycle of fem cycle and subsequent evaluation with the failure criteria is carried on until complete failure. Tension tests can be simulated with such a procedure to figure out the strength of the material. As, this approach uses a set of different failure criteria, it can be used to predict suitability of certain criteria for a particular material in question.

As, will be seen in the next chapter, this approach is used to evaluate the different failure theories for predicting failure in composite materials [24].

2.3. Conclusions

The maximum stress and maximum strain criteria are known to over predict the failure stresses significantly for a lamina and as well as for a laminate [20]. These stress or strain based criteria are employed in many of commercial softwares. These criteria predict the onset of failure. The elements that satisfy these criteria are deleted. Hence the inelastic regime of the composites remains unexplored with the usage of these criteria. On the other hand, the tsai-hill criteria is known to have a better match with the experimental observations for a lamina and as well as for a laminate, in terms of the failure stress prediction.

The Puck's model [21] employs the concept of fracture plane, hence requires the specification of the inclination parameters. The work of Matzenmiller et al. [22], though implemented in the commercial software "Abaqus" can be used only with elements with plane stress formulation.

The work of Camanho et al. [23] uses a multi scale approach to include interlaminar and intralaminar failure mechanisms.

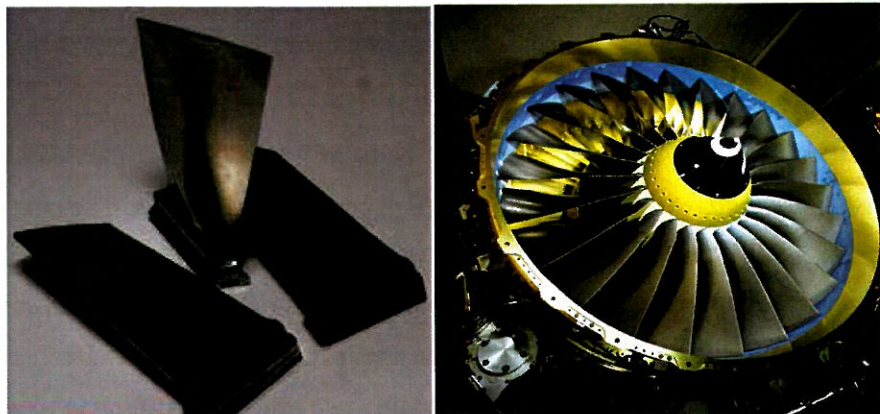
With this, there is a strong need for a body of work which compares and evaluates the state of art failure theories for predicting failure in composite materials. The next chapter focuses on the work carried out to compare the state of art theories for predicting failure in composite materials.

3. Damage prediction with the state of art failure theories

3.1 Introduction

Although there is lot of work done in the past in the field of composite materials and many failure criteria and progressive damage methodologies developed, It could be surprising to note that, there is very little evidence to show that these failure criteria and failure methodologies predict failure accurately and meaningfully for other than a very limited range of conditions [24].

In order to confirm the current state of art of predicting failure in composite laminates, an investigation is made by using commercial software. The investigation involves a simulation of tension test on the root of the fan blade to compare it with the experimental results. The fan blade, shown in figure (3.1) forms part of the compressor in a gas turbine engine, is made up of composite laminate. The commercial software employs the state of art failure criteria to predict failure in composite laminates. This chapter describes the work carried to simulate the tension test on root of fan blade with description of the software.

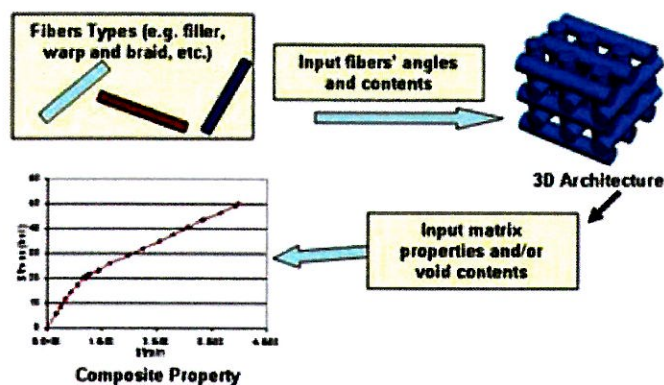


(Figure 3.1- Fan blade on left and the jet engine with composite fan blades on the right. After
“[www . compositeworld.com](http://www.compositeworld.com)”)

3.2. A brief about the software

3.2.1. Material parameter calculation

The software employed in this investigation adopts the micro and macro mechanics methodology. The software formulates the composite properties based on the constituent properties, which forms the basis for the micromechanics approach. Then the composite properties are integrated to form the overall stiffness for finite element analysis.

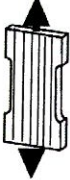

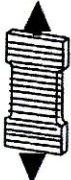
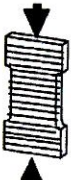



(Figure 3.2-Scheme adopted to calculate the mechanical and physical properties. After [24])

The figure (3.2) shows the composite micromechanics scheme used by the software. The fiber properties with its orientation angles are needed, in order to calculate the composite properties. These properties of the fiber when combined with matrix properties along with the fiber volume fractions yield the properties of the composite. The following properties of the composite are calculated: stiffness, Poisson's ratios, strengths, coefficients of thermal expansion, and coefficients of hygral expansion, heat conductivities, and moisture diffusivities.

The in plane properties are obtained by carrying out tension and compression tests along the longitudinal and the transverse directions as in figure (3.3) below. While doing so, care should be taken to specify the boundary conditions and contact conditions accurately [25].

On, the other hand, the same process can be adopted to conduct the inverse modeling i.e., the properties of the matrix and the reinforcement can be adjusted to gain the desired laminate properties, thereby arriving at the desired matrix and fiber properties.

Test Type				
3 coupons Longitudinal Tension	3 coupons Longitudinal Compression	3 coupons Transverse Tension	3 coupons Transverse Compression	3 coupons Shear
				
ASTM D638, D3039	ASTM D695, D3410	ASTM D638, D3039	ASTM D695, D3410	ASTM D3518

(Figure 3.3-Tests to calculate the mechanical properties. After [24])

3.2.2. A brief about the failure criteria employed by the software

The commercial software employs the state of art criteria to evaluate failure in composite laminates. The failure criteria employed by the software can be broadly classified as strength based criteria and interactive criteria.

The following criteria fall in the group of strength based criteria: Longitudinal tensile strength, Longitudinal compression, Transverse Tensile, Transverse compression, In plane shear(+), In plane shear (-), Normal Tension, Normal compression, Transverse out of plane shear(+), Transverse out of planes shear(-), Longitudinal out of plane shear(+), Longitudinal out of plane shear(-) and Relative Rotation [26].

The following criteria fall in the group of interactive criteria: Tsai- Wu, Tsai-Hill, Modified distortion energy and Puck.

Table (3.1) gives the list of strength based criteria along with a description of each of them.

STRENGTH BASED CRITERIA	DESCRIPTION
Longitudinal tensile (S11T)	This is based on the fiber strength and the fiber volume fraction.
Longitudinal compressive (S11C)	This is based on the fiber compressive strength and the fiber volume fraction.
Transverse tensile (S22T)	This is based on the matrix modulus, matrix tensile strength and fiber volume fraction.
Transverse tensile (S22C)	This is based on the matrix modulus, matrix compressive strength and fiber volume fraction.
Normal tensile (S33T)	This predicts the ply separation.
Normal compression (S33C)	This is used to predict the crushing of the laminate.
Positive -In plane shear (S12)	This is based on the in plane shear strength.
Negative -In plane shear (S12)	This is based on the in plane shear strength.
Positive transverse normal shear (S23)	This is based on the shear strength in transverse normal plane.
Negative -transverse normal shear (S23)	This is based on the shear strength in transverse normal plane.
Positive longitudinal normal shear (S13)	This is based on the shear strength in longitudinal normal plane.
Negative -longitudinal normal shear (S13)	This is based on the shear strength in longitudinal normal plane.
Relative rotation	This is based on the maximum rotation allowed by the plies.

(Table 3.1-List of strength based criteria with its description)

Among this, the following criteria are believed to predict delamination accurately: Normal tension, Transverse out of plane shear(+), Transverse out of plane shear(-), Longitudinal out of plane shear(+), Longitudinal out of plane shear(-) and Relative Rotation.

The interactive criteria employed by the software are expressed as follows [26]:

Modified Distortion Energy Criteria: this criterion is expressed as in Equation (3.1).

$$F = 1 - \left[\left(\frac{\sigma_{L11}}{S_{L11}} \right)^2 + \left(\frac{\sigma_{L22}}{S_{L22}} \right)^2 - K_{L12} \left(\frac{\sigma_{L11}}{S_{L11}} \right) \left(\frac{\sigma_{L22}}{S_{L22}} \right) + \left(\frac{\sigma_{L12}}{S_{L12}} \right)^2 \right] \quad (3.1)$$

Where the directional interaction factor is defined as follows:

$$K_{L12} = \frac{(1+4\nu_{L12}-\nu_{L13})E_{L22} + (1-\nu_{L23})E_{L11}}{\sqrt{E_{L11}E_{L22}(2+\nu_{L12}+\nu_{L13})(2+\nu_{L21}+\nu_{L23})}}$$

Tsai-Hill: this criterion is expressed as in Equation (3.2).

$$F = 1 - \left[\left(\frac{\sigma_{L11}}{S_{L11}} \right)^2 + \left(\frac{\sigma_{L22}}{S_{L22}} \right)^2 - \left(\frac{\sigma_{L11}\sigma_{L22}}{S_{L11}^2} \right) + \left(\frac{\sigma_{L12}}{S_{L12}} \right)^2 \right] \quad (3.2)$$

Tsai-Wu: this criterion is expressed as in Equation (3.3).

$$F = 1 - (f_1\sigma_{L11} + f_2\sigma_{L22} + f_{11}\sigma_{L11}^2 + f_{22}\sigma_{L22}^2 + f_{12}\sigma_{L12}^2 + 2f_{12}\sigma_{L11}\sigma_{L22}) \quad (3.3)$$

$$f_1 = \frac{1}{S_{L11T}} - \frac{1}{S_{L11C}} \quad f_2 = \frac{1}{S_{L22T}} - \frac{1}{S_{L22C}} \quad f_{11} = \frac{1}{S_{L11T}S_{L11C}} \quad f_{22} = \frac{1}{S_{L22T}S_{L22C}} \quad f_{12} = \frac{1}{2}(f_{11}f_{22})^{\frac{1}{2}}$$

3.2.3. Failure prediction

The commercial software employed in this investigation, makes use of a multi-step iterative procedure. In this procedure, the load on the structure is increased in small increments. At each load step, a nonlinear analysis is performed until the solution converges. This converged solution represents an equilibrium state. Then, relative to the equilibrium state, the stresses within each lamina are determined from the nonlinear-analysis solution. These stresses are evaluated with the strength based criteria and the interactive criteria.

If a failure criterion indicates failure of a lamina, then the properties of the lamina are changed according to the kind of failure criteria satisfied. (This is done based on the kind of failure criterion satisfied, the corresponding properties are degraded. For example, if the longitudinal strength criterion is satisfied then the young's modulus of the matrix and fiber are reduced and on other hand, only the young's modulus of the matrix is reduced if transverse strength criterion is satisfied) [24, 25].

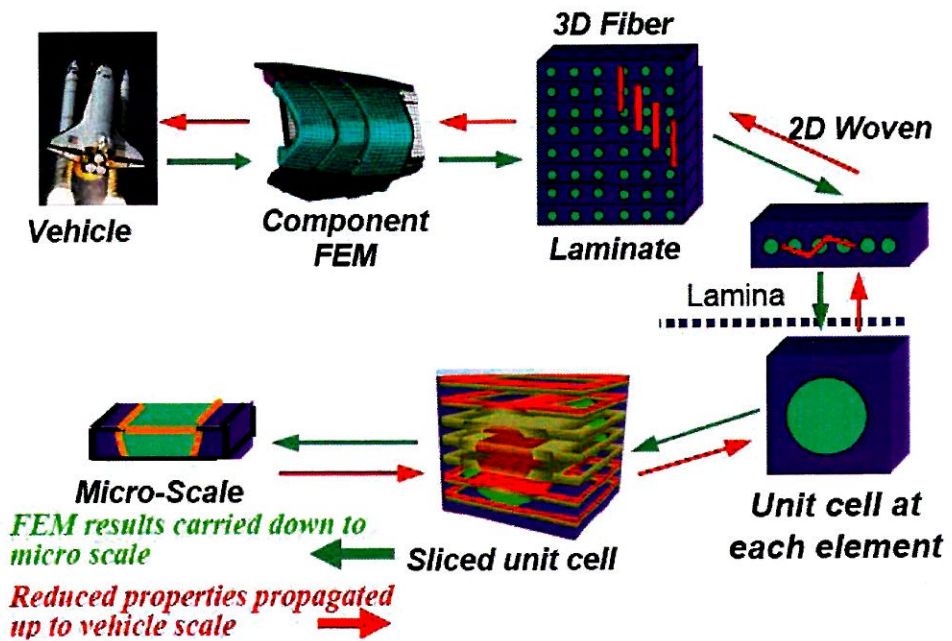
When this happens, the initial nonlinear solution no longer corresponds to an equilibrium state, and it becomes necessary to re-establish equilibrium, using the modified lamina properties for the failed lamina while maintaining the current load level. This iterative process of obtaining nonlinear equilibrium solutions each time a local material sub model is modified is continued until no additional lamina failures are detected. However, because in this progressive failure methodology, small load step sizes were used the need for a second iterative process over the

small step could be eliminated in obtaining equilibrium solutions. The load is incremented and the foregoing analysis repeated until complete failure of the structure is detected.

Computational simulation is achieved by the integration of three distinct modules acting at different scales (micro to macro) into a progressive failure tracking code. The distinct computational modules are: (1) a composite mechanics module, (2) a finite element analysis module, and (3) a damage progression-tracking module.

- (1) The composite mechanics module, as discussed earlier calculates the properties of the composite laminate starting from the properties of the constituents (fiber, matrix and fiber volume fraction).
- (2) The finite element analysis module is generally an external Finite element code, which in this case was Abaqus.
- (3) The damage tracking module takes the solution from the Abaqus solver, makes use of the classical laminate theory to bring to the stresses to lamina level, where they evaluated with a combination of strength based criteria and interactive criteria. The damage tracking is done with the help of binary index. The appropriate properties of the material are reduced based on the failure criteria met and then the overall stiffness property of the structure is recalculated with the composite mechanics module.

As, the loads are applied in increments, the above steps are repeated, until the final load is reached. The entire process of the computational simulation which involves various scales is as shown in figure (3.4) [24, 25].

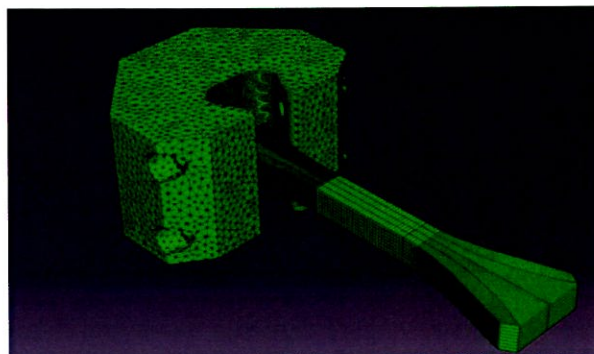


(Figure 3.4-Progression of Failure from lamina to structure. After [24])

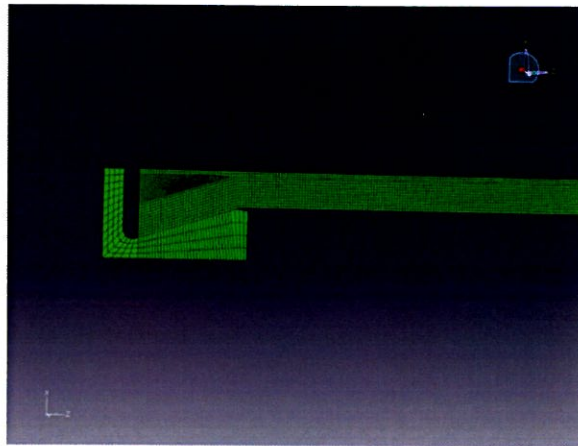
3.3. Description of the analysis carried out

3.3.1. Description of the specimen

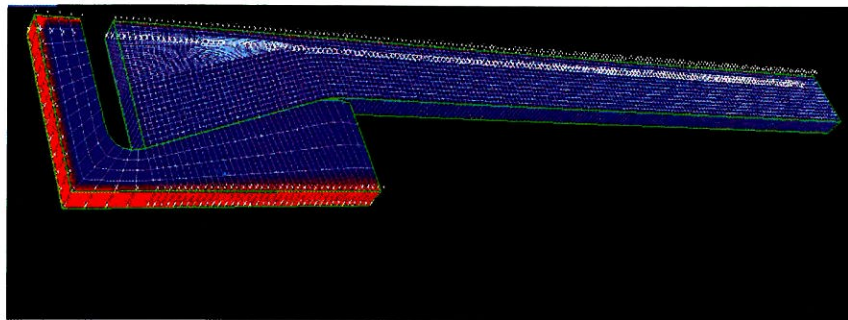
The root of the fan blade is held in the tension wedge grip as shown in the figure (3.5) on one side and the other side is subjected to a displacement. The model due to symmetry reasons is reduced in size to 1/8th of the original model as shown in the figure (3.6).



(Figure 3.5- Complete model)



(Figure 3.6-1/8th model)



(Figure 3.7- Boundary Conditions defined for the specimen)

Coefficient of friction between the contact surfaces (i.e. the surfaces between the specimen and the grip) is specified to be 0.2. The surface highlighted in red in the figure (3.7) is fixed in the x-direction and the end opposite to this surface is given a displacement of 6.5 mm in the x-direction. The model is meshed with 20 node brick elements.

A static analysis is simulated with INITIAL INCREMENT SIZE: 0.1 MINIMUM: 1e-010 MAXIMUM INCREMENT SIZE: 1. To prevent element deletion in the contact region between the specimen and the grip, which might lead to contact errors, the element deletion option is turned off and an artificial stiffness of 0.1 is set in the elements.

3.3.2. Material Parameters and the stacking sequence.

The material parameters of the specimen for one of the plies is as given in the table (3.2)

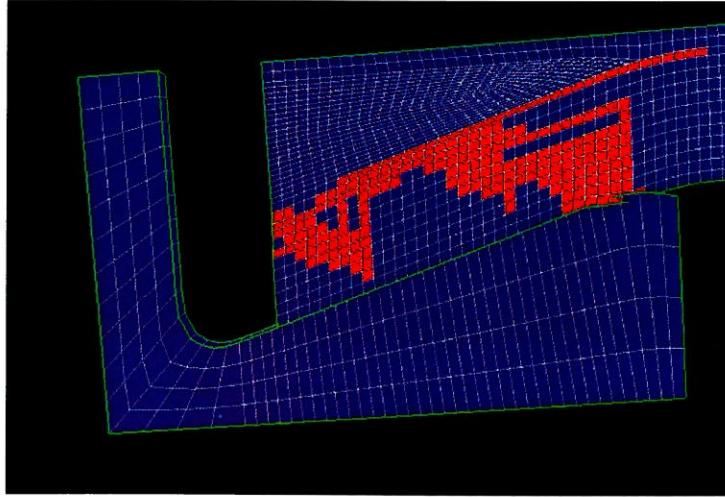
PROPERTY	VALUE	UNITS
E1 (Young's Modulus along the fiber direction)	5.69e4	MPa
E2(Young's Modulus along the first transverse direction)	1.038E+05	MPa
E3(Young's Modulus along the second transverse direction)	1.000E+04	MPa
G12(Shear Modulus in 1-2 direction)	5.900E+03	MPa
G23(Shear Modulus in 2-3 direction)	5.900E+03	MPa
G31(Shear Modulus in 3-1 direction)	3.600E+03	MPa
X11(Tensile Strength along the fiber direction)	6.828E+02	MPa
X22(Tensile Strength along the first transverse direction)	1.246E+03	MPa
X33(Tensile Strength along the second transverse direction)	1.200E+02	MPa
S12(Shear Strength in the 1-2 plane)	7.080E+01	MPa
NU12 (Poisson's ratio)	5.290E-02	-
NU23(Poisson's ratio)	5.272E-02	-
NU13(Poisson's ratio)	1.644E-01	-
Density	1.542E-09	Ton/mm ³
EPST1(Tensile strain limit)	1.200E-02	-
EPS1C (Compressive strain limit)	1.200E-02	-
EPS1S (Shear strain limit)	1.200E-02	-

(Table 3.2-List of properties defined for one the plies of the specimen)

3.4. Results

The following damages patterns were observed in the root specimen using a combination of each of the different interactive criteria and the strength based criteria:

- Modified distortion energy:



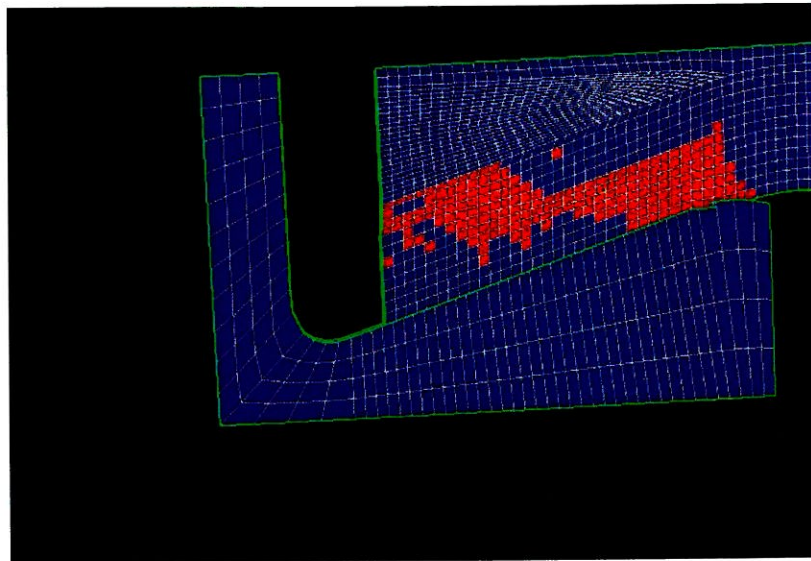
(Figure 3.8- Damage pattern predicted by Modified distortion energy criteria)

The figure (3.8) shows the damage pattern predicted by the combination of strength based criteria and modified distortion energy criteria. The elements in red are the ones which are damaged. At least one ply in each of these damaged elements has satisfied at least one of the criteria.

Firstly damage begins as shear bands at the region of contact between the specimen and the grip of tension testing machine and then delamination begins at the tip of the specimen and grows along the length of the specimen.

This prediction by the software is in contrast to the experimental observation, wherein damage initiates as delamination at the tip of the specimen and grows along the length of the specimen and later on progresses as shear bands in the contact region between the specimen and the holding device.

- Puck's criteria:



(Figure 3.9- Damage pattern predicted by Puck's criteria)

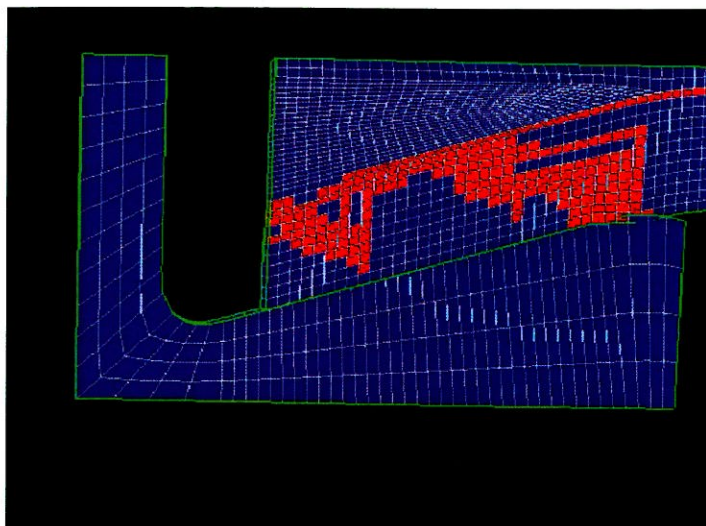
The figure (3.9) shows the damage pattern predicted by the strength based criteria and Puck criteria. The elements in red are the ones which are damaged. At least one ply in each of these damaged elements has satisfied at least one of the criteria.

Firstly damage begins as shear bands at the region of contact between the specimen and the holding device of Tensile testing machine and then delamination begins at the tip of the specimen and grows along the length of the specimen.

This prediction by the software is in contrast to the experimental observation, wherein damage initiates as delamination at the tip of the specimen and grows along the length of the specimen and later on progresses as shear bands in the contact region between the specimen and the holding device.

- Tsai-Hill:

The figure (3.10) shows the damage pattern predicted by the combination strength based criteria and Tsai-Hill. The elements in red are the ones which are damaged. At least one ply in each of these damaged elements has satisfied at least one of the criteria.

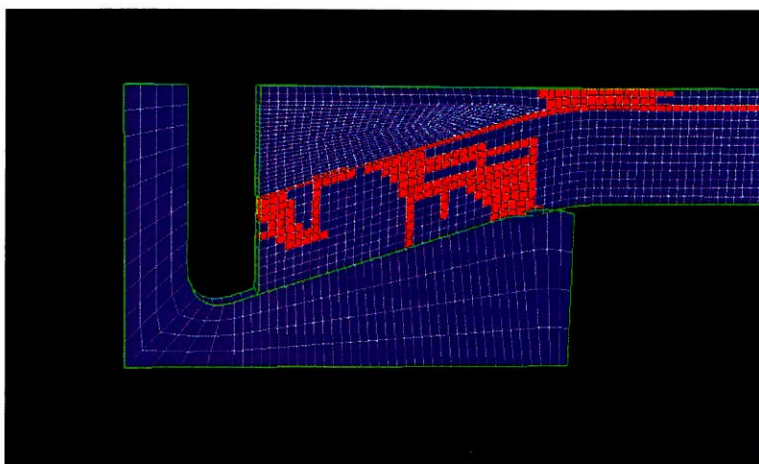


(Figure 3.10- Damage pattern predicted by Tsai-Hill criteria)

Firstly damage begins as shear bands at the region of contact between the specimen and the holding device of Tensile testing machine and then delamination begins at the tip of the specimen and grows along the length of the specimen.

This prediction by the software is in contrast to the experimental observation, wherein damage initiates as delamination at the tip of the specimen and grows along the length of the specimen and later on progresses as shear bands in the contact region between the specimen and the holding device.

- Tsai-Wu:



(Figure 3.11- Damage pattern predicted by Tsai-Wu criteria)

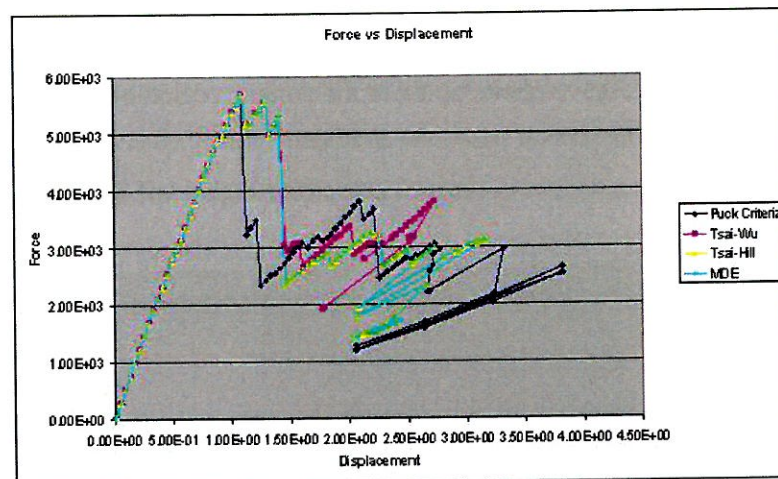
The figure (3.11) shows the damage pattern predicted by the strength based criteria and Tsai-Wu. The elements in red are the ones which are damaged. At least one ply in each of these damaged elements has satisfied at least one of the criteria.

Firstly damage begins as shear bands at the region of contact between the specimen and the holding device of Tensile testing machine and then delamination begins at the tip of the specimen and grows along the length of the specimen.

This prediction by the software is in contrast to the experimental observation, wherein damage initiates as delamination at the tip of the specimen and grows along the length of the specimen and later on progresses as shear bands in the contact region between the specimen and the holding device.

3.4.1. Plot of force displacement curve

Force displacement diagrams as shown in figure (3.12) is plotted considering one of the nodes of the fan blade root specimen which is subjected to a non-zero displacement.



(Figure 3.12-Comparison of the force displacement diagram for various interactive criteria)

3.5 Conclusions

From the above plots of the damage patterns, it can be concluded that the damage pattern predicted by the each of the following criteria: MDE, Tsai-Hill, Tsai-Wu in combination with the strength based criteria is more less the same as their expressions are more less similar. The damage pattern in Puck criteria is different from the rest, as in the formulation adopted for Puck criteria, only fiber and inter fiber damage is taken into account.

From the force displacement diagram, it can be observed that the failure stress predicted by these criteria (combination of strength based criteria and interactive criteria) is much lower than what is observed in the experiments and hence the failure stress predicted is very conservative.

To sum up, Failure in composite structures is a complex phenomenon. Basically, as a function of the load spectra, the failure process gradually proceeds by reducing stiffness and strength, and reconfiguring the load distribution. Although many failure criteria and progressive damage methodologies are presented in the literature, there is as yet no universal failure model for composite material/structure.

The available present day commercial softwares used by the leading aircraft industries such as Rolls-Royce make use of a combination of stress based criteria (most of which are mere extensions of the isotropic yield criteria) and progressive damage methodology to predict failure. But the damage initiation and propagation of damage predicted by such softwares are found to be in contrast with the experimental results.

Utilization of advanced composite materials to their full potential requires establishment of accurate damage models. Therefore, there is a need for a model which accurately represents the behavior of the composite material. The aim of this thesis is towards implementation of one such damage model [1], which models the non linear stress-strain behavior after failure initiation in a three dimensional framework, in Abaqus sub routine (VUMAT).

4. Implementation of the Damage Model

4.1. Introduction

The implemented damage model is a three dimensional mixed mode damage model that describes the elastic-brittle behavior of the fiber reinforced composite laminates. This model was proposed by J.L.Curiel Sosa et al. (2008) [1]. Implementation and further modifications are conducted at the presented research.

The composite laminate is considered as a homogenized continuum and the constitutive law is defined using an orthotropic constitutive tensor. The damage model takes into account the damage modes in composites such as fiber rupture, fiber kinking, matrix cracking and matrix crushing by the use of damage variables. The damage variables that are the internal variables describe the evolution of damage state under loading and as a subsequence the degradation of the material stiffness.

The evolution of damage variables ensures suitable coupling between the various damage modes by the use of directional vectors and hence giving rise to the mixed mode nature of the model.

4.2. Assumptions

The following assumptions are made in the development of the model:

- The theoretical basis for the constitutive model of each UD-laminate is provided by a homogenized continuum.
- The rules of mixtures lead to the elasticity moduli and strength parameters of the undamaged UD-laminate, calculated from the properties of fiber and resin data together with the volume ratios of fibers and matrix.
- The laminate is assumed to have an elastic behavior which is linear, when loaded in tension or compression, until the initiation of damage. Once the damage initiates the

behavior is assumed to be non-linear. The non-linear behavior is controlled by the damage variables.

- The orthotropic nature of the lamina as a homogenized continuum is maintained throughout the damaging process. This means: the defects in the composite material are treated in the mathematical model as having the equivalent effect on the elastic properties as disk-like cracks would exert, if they are only oriented either tangential or normal to the fiber direction. Therefore, the symmetry class of the UD-laminate remains the same for all states of damage.
- After an initial elastic behavior, there is rearrangement of material properties due to progressive damage.

4.3. The description of the model

The model involves the definition of six damage internal variables ω_{kj} included into the damage tensor \mathbf{D} as in equation (4.1)-that represents the state of damage in the composite.

$$\hat{\sigma} = \mathbf{D} \cdot \sigma \quad (4.1)$$

Where

$$\sigma^T = [\sigma_{11}, \sigma_{22}, \sigma_{33}, \sigma_{12}, \sigma_{23}, \sigma_{31}]$$

is an array formed by the stress components and is the so-called effective stress [27]. It is assumed that the tensors and properties are defined in a local system of reference for the UD-lamina. Thus, in a local system of references, 1 corresponds to direction parallel to the fibers and the index 2 corresponds to the first transverse direction and 3 correspond to the second transverse direction.

$$\mathbf{D} = \text{diag} \left[\frac{1}{1-\omega_{11}}, \frac{1}{1-\omega_{22}}, \frac{1}{1-\omega_{33}}, \frac{1}{1-\omega_{12}}, \frac{1}{1-\omega_{23}}, \frac{1}{1-\omega_{31}} \right] \quad (4.2)$$

The damage tensor D is formed as a diagonal tensor and contains the damage internal variables, see Equation (4.2). These internal variables (which take values between 0 and 1) play a role in degrading the stiffness properties. The effective stresses are assumed to fulfill the strain equivalence principle through Equation (4.3) [28].

$$\hat{\sigma} = C_0 \cdot \varepsilon \quad (4.3)$$

where C_0 is the undamaged stiffness matrix. C denotes the so-called 'damaged' constitutive tensor. It is clear from the definition of C that the introduction of the damage internal variables renders a non-symmetric tensor, see Equation (4.4).

$$\sigma = D^{-1} \cdot C_0 \cdot \varepsilon = C(\omega) \cdot \varepsilon \quad (4.4)$$

The matrices A and B defined in a local system of reference are introduced in order to read C in a more compact manner.

$$A(\omega) = \begin{bmatrix} \frac{(1-\omega_{11})(1-\nu_{23} \nu_{32})}{E_{22} E_{33} \Delta} & \frac{(1-\omega_{11})(\nu_{12} + \nu_{32} \nu_{13})}{E_{11} E_{33} \Delta} & \frac{(1-\omega_{11})(\nu_{13} + \nu_{12} \nu_{23})}{E_{22} E_{33} \Delta} \\ \frac{(1-\omega_{22})(\nu_{12} + \nu_{32} \nu_{13})}{E_{11} E_{33} \Delta} & \frac{(1-\omega_{22})(1-\nu_{13} \nu_{31})}{E_{11} E_{33} \Delta} & \frac{(1-\omega_{22})(\nu_{23} + \nu_{21} \nu_{13})}{E_{11} E_{22} \Delta} \\ \frac{(1-\omega_{33})(\nu_{13} + \nu_{12} \nu_{23})}{E_{11} E_{22} \Delta} & \frac{(1-\omega_{33})(\nu_{23} + \nu_{21} \nu_{13})}{E_{11} E_{22} \Delta} & \frac{(1-\omega_{33})(1-\nu_{12} \nu_{21})}{E_{11} E_{22} \Delta} \end{bmatrix} \quad (4.5)$$

With

$$\Delta = \frac{(1 - \nu_{12} \nu_{21} - \nu_{23} \nu_{32} - \nu_{31} \nu_{13} - 2\nu_{21} \nu_{32} \nu_{13})}{E_{11} \cdot E_{22} \cdot E_{33}}$$

$$B(\omega) = \begin{bmatrix} (1 - \omega_{11})G_{12} & 0 & 0 \\ 0 & (1 - \omega_{11})G_{23} & 0 \\ 0 & 0 & (1 - \omega_{11})G_{31} \end{bmatrix} \quad (4.6)$$

Taking into account Equations (4.5-4.6), the damaged constitutive tensor can be written in a more compact manner as in, Equation (4.7).

$$C(\omega) = \begin{bmatrix} A(\omega) & 0 \\ 0 & B(\omega) \end{bmatrix} \quad (4.7)$$

4.3.1 Evolution of damage

The damage model takes into account the following damage modes: fiber rupture, fiber kinking, matrix cracking and matrix crushing. These types are modeled by means of a combination of growth functions Φ_γ for a particular mode of damage γ and damage directors $\mathbf{v}^{(\gamma)}$. Thus, the damage rule is defined as a linear combination of the growth functions and the damage directors, Equation (4.8).

$$\dot{\omega} = \sum_{\gamma=1}^{nmodes} \Phi_\gamma \mathbf{V}^{(\gamma)} \quad (4.8)$$

In the above equation, “nmodes” denotes the total number of failure modes. The growth functions for each damage mode are computed through Equation (4.9).

$$\Phi_{(\gamma)} = \langle \nabla_\varepsilon g^{(\gamma)} / \|\nabla_\varepsilon g^{(\gamma)}\|, \dot{\varepsilon} \rangle_+ \quad (4.9)$$

where $\langle \cdot, \cdot \rangle_+$ is the non-negative inner product -vanishing for negative values- accounting for the trespassing on the damage surface. This ensures that there is no growth of damage if the damage surface is not reached. If the strain increment vector is pointing to the interior of the surface, for a generic damage mode, there is no progression of that particular damage mode. So a simple way to effectively compute this is to perform the nonnegative scalar product as represented in Equation (4.9). In Equation (4.9), the strain rate dependence is included. g are the evolving damage surfaces in the strain space defined in Equation (4.10).

$$g^{(\gamma)} = \varepsilon^T \cdot \mathbf{G}^{(\gamma)} \cdot \varepsilon - c^{(\gamma)} \quad (4.10)$$

where c^γ is an empirical parameter defining the damage surface. The variations of these surfaces on the strain space render Equation (4.11).

$$\mathbf{V}_\varepsilon g^{(\gamma)} = \varepsilon^T \cdot (\mathbf{G}^{(\gamma)T} + \mathbf{G}^{(\gamma)}) \quad (4.11)$$

where \mathbf{G} are obtained from the constitutive law -Equation (4.4)- and from the equivalence of the quadratic forms in stress and strain spaces [28] given by Equation (4.12).

$$\sigma^T \cdot \mathbf{F}^{(\gamma)} \cdot \sigma = \varepsilon^T \cdot \mathbf{G}^{(\gamma)} \cdot \varepsilon \quad (4.12)$$

The \mathbf{F} - second-order tensors are derived from stress-based criteria of failure with the introduction of the damage internal variables as shown in reference [29]. The modeling of the unitary damage

directors \mathbf{v} is based upon the stiffness components that are degraded when a particular mode of damage occurs. For instance, fiber rupture \mathbf{v}^1 affects to the stiffness degradation in (11), (12) and (31) directions, Equation (4.13).

$$\mathbf{v}^{(1)} = \left[\lambda_{11}^{(1)} \ 0 \ 0 \ \lambda_{12}^{(1)} \ 0 \ \lambda_{21}^{(1)} \right]^T \quad (4.13)$$

The weights λ are estimated taking into account the experimental observations for that particular mode of failure. This approach admits inverse modeling to better adaptation to the physical response but this has not been attempted at this time.

Regarding the implementation of the model, it should be mentioned that it is better adapted for explicit finite element methods or combined implicit-explicit methods [30].

4.4. Formulation implemented in Abaqus VUMAT

The strain increment is passed on, into the VUMAT subroutine from Abaqus [31], along with the damage variables calculated in the previous time step. Following which,

The new strain: $\boldsymbol{\varepsilon}^{N+1}$ is calculated as shown in equation (4.14)

$$\boldsymbol{\varepsilon}^{N+1} = \boldsymbol{\varepsilon}^N + \Delta \boldsymbol{\varepsilon} \quad (4.14)$$

The new stress: $\boldsymbol{\sigma}^{N+1}$ is calculated as shown in equation (4.15)

$$\boldsymbol{\sigma}^{N+1} = \mathbb{C}(\omega) \cdot \boldsymbol{\varepsilon}^{N+1} \quad (4.15)$$

The surface in stress space: \mathbb{F}^{N+1} with the stress in the current time step, as in equation (4.16-4.18) below.

$$\mathbb{F}_{\parallel}^{N+1} = \frac{\sigma_{11}^2}{(1-\omega_{11})^2 \cdot X_{11}^2} + \frac{\sigma_{12}^2}{(1-\omega_{12})^2 \cdot X_{12}^2} + \frac{\sigma_{31}^2}{(1-\omega_{31})^2 \cdot X_{31}^2} \quad (4.16)$$

$$\mathbb{F}_{\perp}^{N+1} = \frac{\sigma_{22}^2}{(1-\omega_{22})^2 \cdot X_{22}^2} + \frac{\sigma_{12}^2}{(1-\omega_{12})^2 \cdot X_{12}^2} + \frac{\sigma_{23}^2}{(1-\omega_{23})^2 \cdot X_{23}^2} \quad (4.17)$$

$$\mathbb{F}_{\perp\perp}^{N+1} = \frac{\sigma_{33}^2}{(1-\omega_{33})^2 \cdot X_{33}^2} + \frac{\sigma_{31}^2}{(1-\omega_{31})^2 \cdot X_{31}^2} + \frac{\sigma_{23}^2}{(1-\omega_{23})^2 \cdot X_{23}^2} \quad (4.18)$$

The surface in strain space: \mathbb{G}^{N+1} is calculated as in equation (4.19)

$$\mathbb{G}^{N+1} = \mathbb{C}(\omega)^T \cdot \mathbb{F} \cdot \mathbb{C}(\omega) \quad (4.19)$$

The gradient to strain surface: $\nabla_{\varepsilon} g$ is calculated as in equation (4.20)

$$\nabla_{\varepsilon} g = \varepsilon^{N+1} \cdot ((\mathbb{G}^{N+1})^T + \mathbb{G}^{N+1}) \quad (4.20)$$

The growth function: φ^{N+1} is calculated as in equation (4.21)

$$\varphi^{N+1} = \dot{\varepsilon}^{N+1} \cdot \nabla_{\varepsilon} g \quad (4.21)$$

The evolution of damage variables: $\dot{\omega}^{N+1}$ is calculated as in equation (4.22)

$$\dot{\omega}^{N+1} = \varphi^{N+1} \cdot \eta \quad (4.22)$$

The updated damage variables: ω^{N+1} is calculated as in equation (4.23)

$$\omega^{N+1} = \dot{\omega}^{N+1} \cdot \Delta t \quad (4.23)$$

The accumulation of damage: ω is calculated as in equation (4.24)

$$\omega = \omega + \omega^{N+1} \quad (4.24)$$

4.5. Tension Test along the fiber direction with one element with one gauss point

The above formulation was implemented in abaqus using the VUMAT subroutine. The subroutine was then used to predict the damage in the cube modeled with one element.

- The cube with a side of 40 mm.
- The following material properties (Table 4.1) were assigned to the composite material:

PROPERTY	VALUE	UNITS
Density	1.52e-9	Ton/mm ³
E1(Young's Modulus along the fiber direction)	126000	MPa
E2(Young's Modulus along the first transverse direction)	11000	MPa
E3(Young's Modulus along the second transverse direction)	11000	MPa
G12(Shear Modulus in 1-2 direction)	6600	MPa
G23(Shear Modulus in 2-3 direction)	3930	MPa

G31(Shear Modulus in 3-1 direction)	6600	MPa
X11(Tensile Strength along the fiber direction)	1950	MPa
X22(Tensile Strength along the first transverse direction)	1950	MPa
X33(Tensile Strength along the second transverse direction)	1950	MPa
S12(Shear Strength in the 1-2 plane)	79	MPa
S23(Shear Strength in the 2-3 plane)	17.14	MPa
S31(Shear Strength in the 3-1 plane)	79	MPa
NU12 (Poisson's ratio)	0.28	-
NU21(Poisson's ratio)	0.024	-
NU23(Poisson's ratio)	0.4	-
NU32(Poisson's ratio)	0.4	-
NU31(Poisson's ratio)	0.024	-
NU13(Poisson's ratio)	0.28	-

(Table 4.1- Table listing the properties specified for the composite laminate)

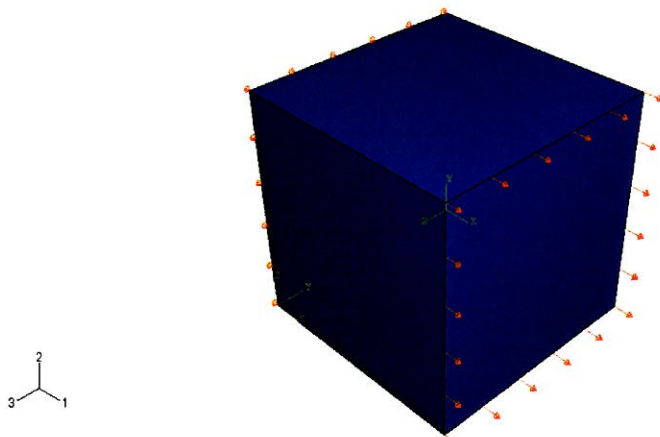
- Explicit Dynamic step

An explicit solver making use of explicit central difference method is selected with non-linear geometry enabled for the problem, with a step time of 1 second.

- Boundary Conditions

The boundary conditions for the cube are defined as follows:

One surface of the cube is fixed along the direction "1" and a displacement of 10mm is specified at the opposite side as show in the figure (4.1).



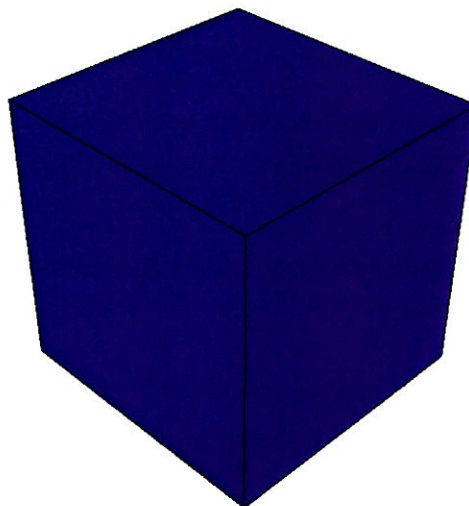
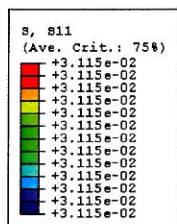
(Figure 4.1- Boundary Conditions specified on the cube)

- Mesh

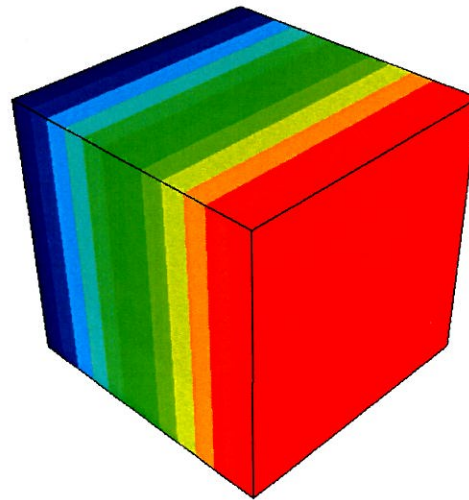
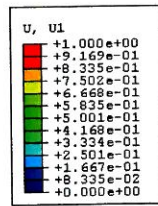
The cube is meshed with one 8-node brick element (reduced integration).

4.5.1. Results

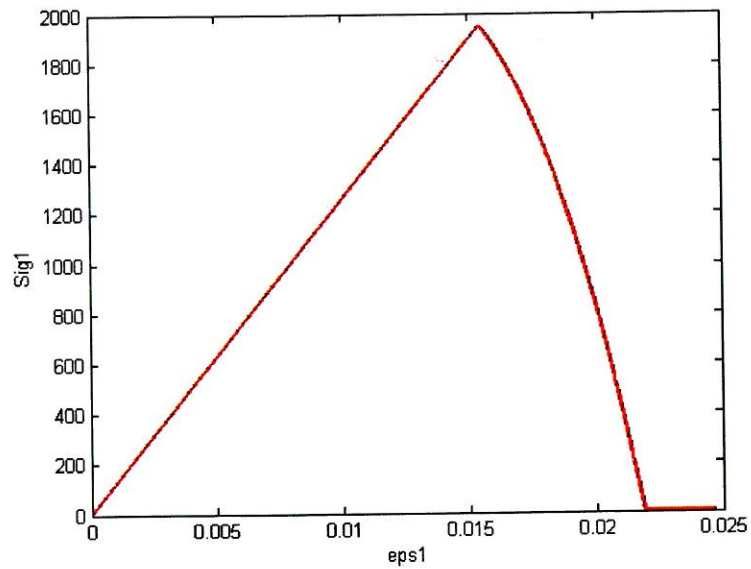
The stresses and displacements along the fiber direction in the last time step are as shown in the figure (4.2) and (4.3) respectively.



(Figure 4.2- Stress -S11 distribution in the cube at the end of the step)

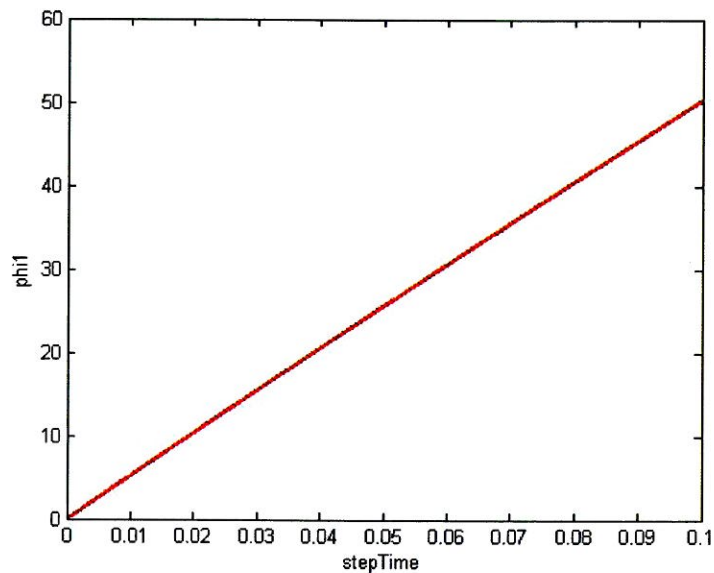


(Figure 4.3- Displacement U1 in the cube)



(Figure 4.4- Stress Strain curve for the cube for tension along the fiber direction)

The figure (4.4) shows the variation of stress along the fiber direction with the strain in the same direction and the figure (4.5) shows the variation of the damage growth function over time for the fiber rupture.



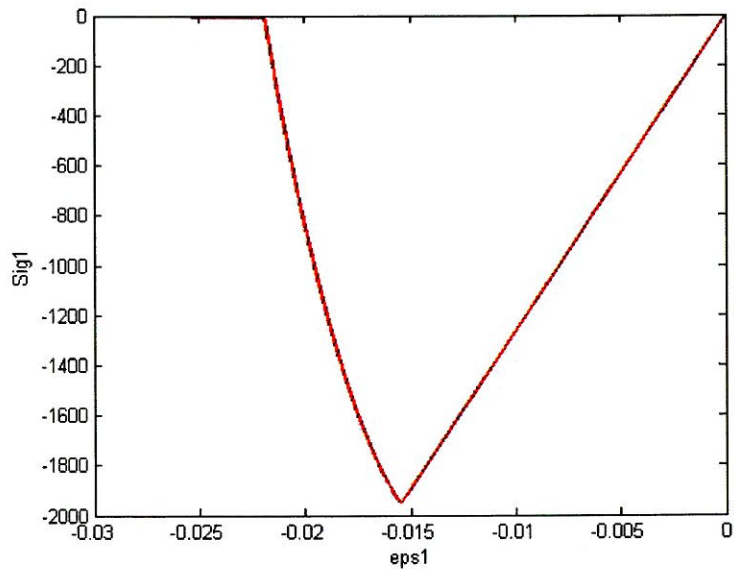
(Figure 4.5- Variation of damage growth function for fiber rupture)

4.6. Compression test along the fiber direction on a cube with one element with one gauss point

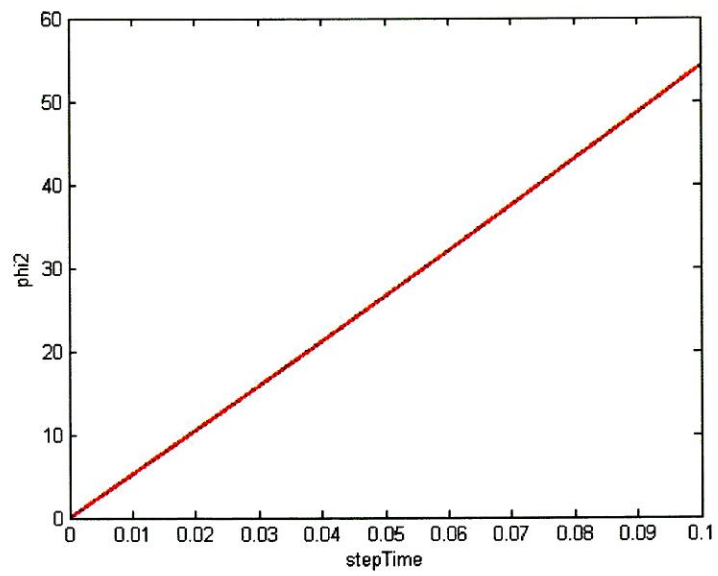
The analysis is set up as it is done for the tension test, except for the compression loading, defined as a displacement specified in the direction opposite to the previous case.

4.6.1. Results for the compression test

The figure (4.6) shows the variation of stress along the fiber direction with the strain in the same direction and the figure (4.7) shows the variation of the damage growth function for the fiber buckling.



(Figure 4.6 – Stress-Strain curve for the cube for compression along the fiber direction)

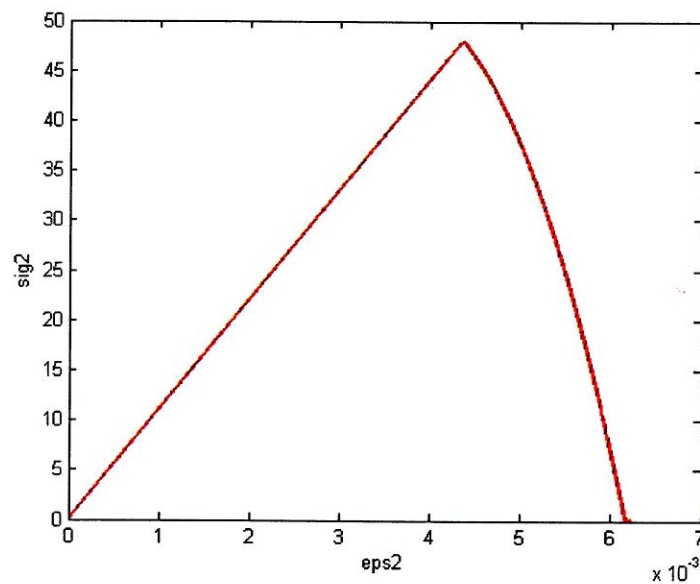


(Figure 4.7 – Variation of damage growth function for fiber buckling)

4.7. Tension test along the first transverse direction on a cube with one element with one gauss point

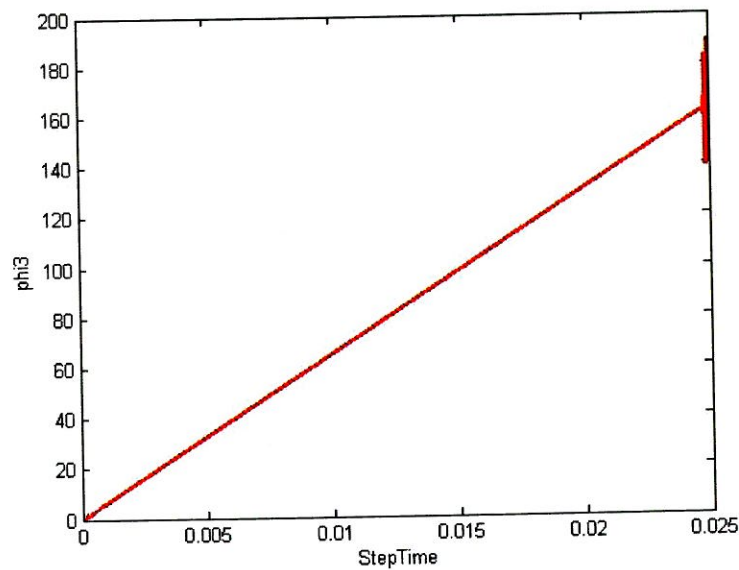
The analysis is set up as it is done for the tension test along the fiber direction, except for the boundary conditions and total time, which is 0.025 s in this case. The boundary conditions have been specified appropriately such that a displacement is specified in the transverse direction.

4.7.1. Results for the Tension test



(Figure 4.8 – Stress Strain curve for the cube for tension along the first transverse direction)

The figure (4.8) shows the variation of stress along the first transverse direction with the strain in the same direction and the figure (4.9) shows the variation of the damage growth function over time for the matrix cracking in the first transverse direction.



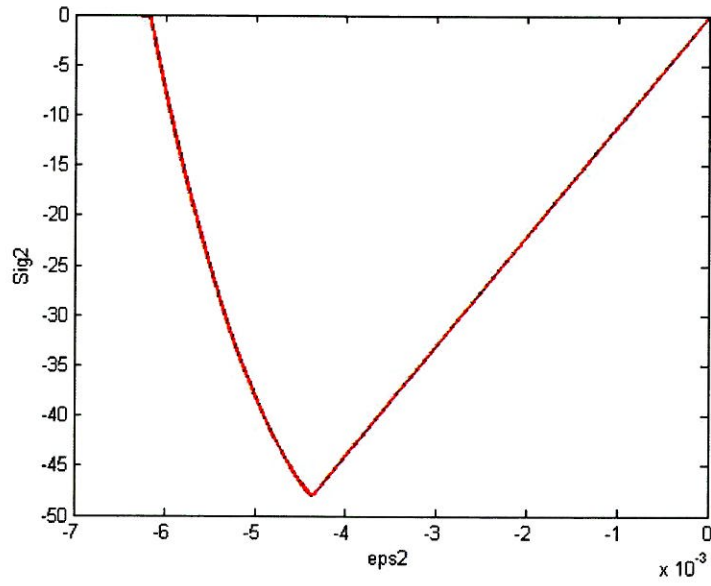
(Figure 4.9 –Variation of the damage growth function for matrix cracking in the first transverse direction)

4.8. Compression test along the first transverse direction on a cube with one element with one gauss point

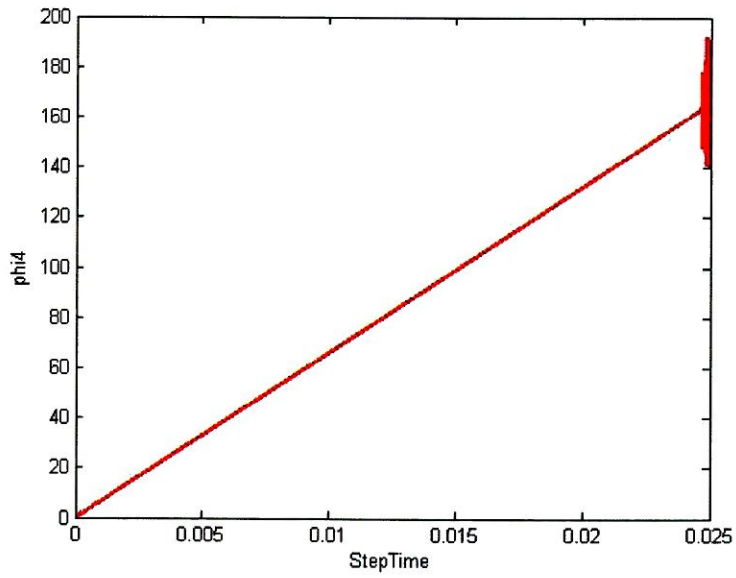
The analysis is set up as it is done for the tension test along the first transverse direction, except for the boundary conditions. The boundary conditions have been specified just as in the case of the tension test along the first transverse direction, except for the non-zero displacement. The non-zero displacement boundary condition is specified such that there is compression along the first transverse direction.

4.8.1. Results for the compression test

The figure (4.10) shows the variation of stress along the first transverse direction with the strain in the same direction and the figure (4.11) shows the variation of the damage growth function over time for the matrix cracking in the first transverse direction.



(Figure 4.10 – Stress-Strain curve for the cube for compression along the first transverse direction)



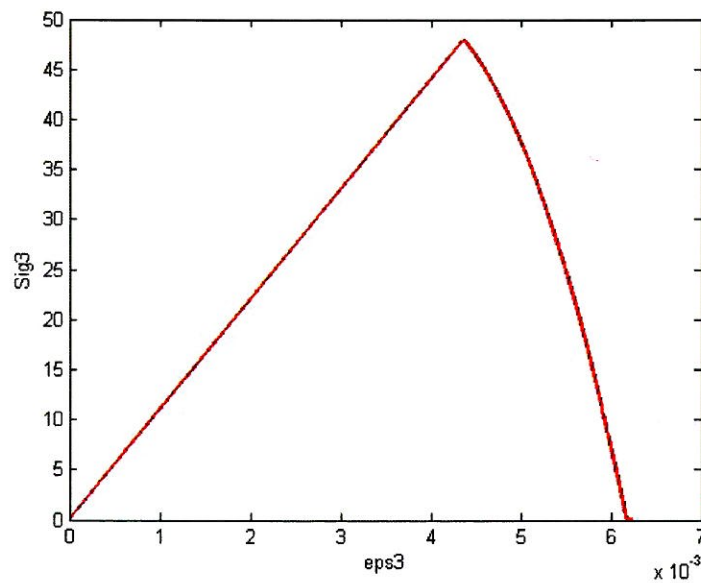
(Figure 4.11 – Variation of the damage growth function for matrix crushing in the first transverse direction)

4.9. Tension test along the second transverse direction on a cube with one element with one gauss point

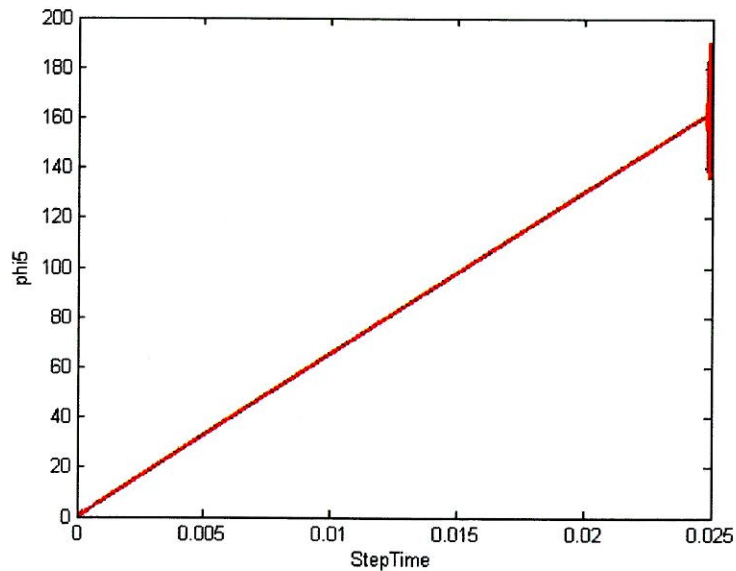
The analysis is set up as it is done for the tension test, except for the boundary conditions.

4.9.1. Results for the Tension test

The figure (4.12) shows the variation of stress along the first transverse direction with the strain in the same direction and the figure (4.13) shows the variation of the damage growth function over time for the matrix cracking in the first transverse direction.



(Figure 4.12 –Stress strain curve for the cube for tension in the second transverse direction)



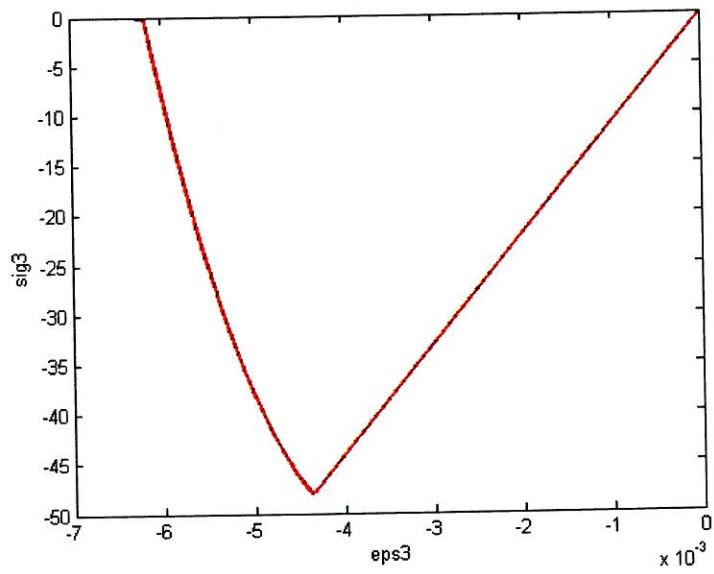
(Figure 4.13 –Variation of damage growth function for matrix cracking in the second transverse direction)

4.10. Compression test along the second transverse direction on a cube with one element with one gauss point

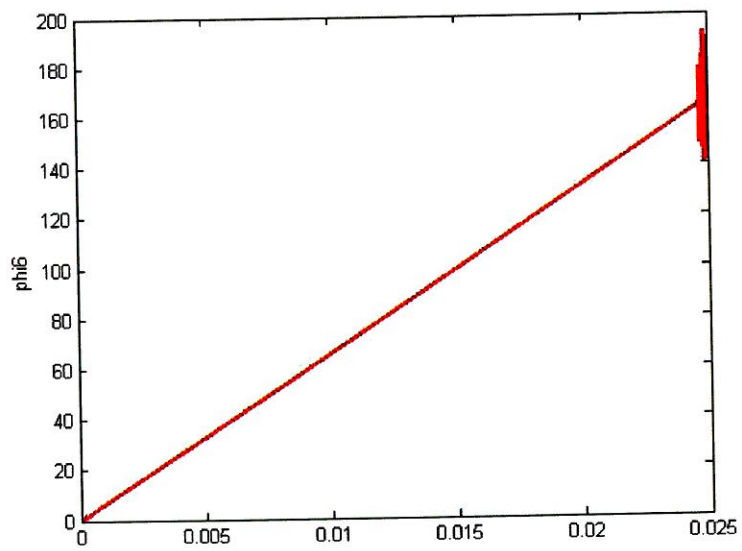
The analysis is set up as it is done for the tension test, except for the compression loading, defined as displacement specified in the direction opposite to the previous case.

4.10.1. Results for the Tension test

The figure (4.14) shows the variation of stress along the first transverse direction with the strain in the same direction and the figure (4.15) shows the variation of the damage growth function over time for the matrix crushing in the second transverse direction.



(Figure 4.14 –Stress-strain curve for the cube for compression in the second transverse direction)



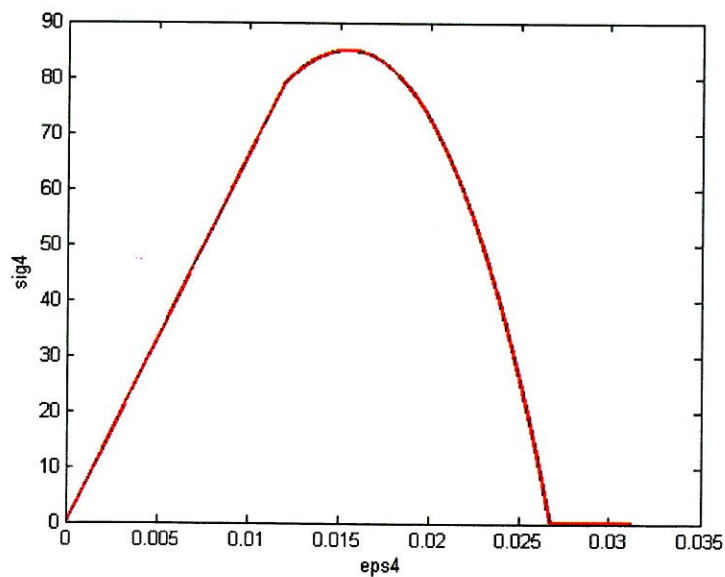
(Figure 4.15 –Variation of growth function for matrix crushing in the second transverse direction)

4.11. Shear Stress-Strain relationship in 12 Plane

The analysis is set up such that there is positive shear in the 12 plane i.e., a positive in plane shear is defined for the composite laminate.

4.11.1. Results for the in plane shear test

The figure (4.16) shows the variation of in-plane stress with in-plane strain in the 12 plane.



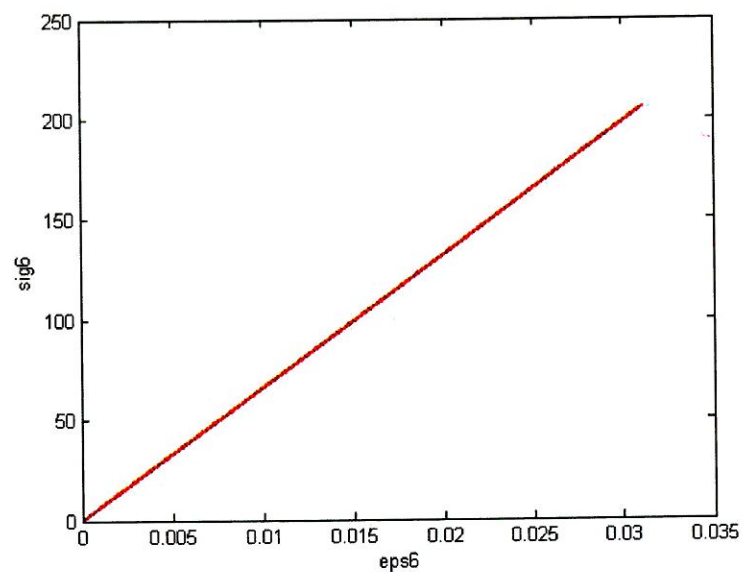
(Figure 4.16 –Stress strain curve for the cube for shear in the 1-2 plane)

4.12. Shear Stress-Strain relationship in 13 Plane

The analysis is set up such that there is positive shear in the 13 plane i.e., a positive longitudinal out of plane shear is defined for the composite laminate.

4.12.1. Results for the longitudinal out of plane shear test

The figure (4.17) shows the variation of in-plane stress with in-plane strain in the 13 plane.



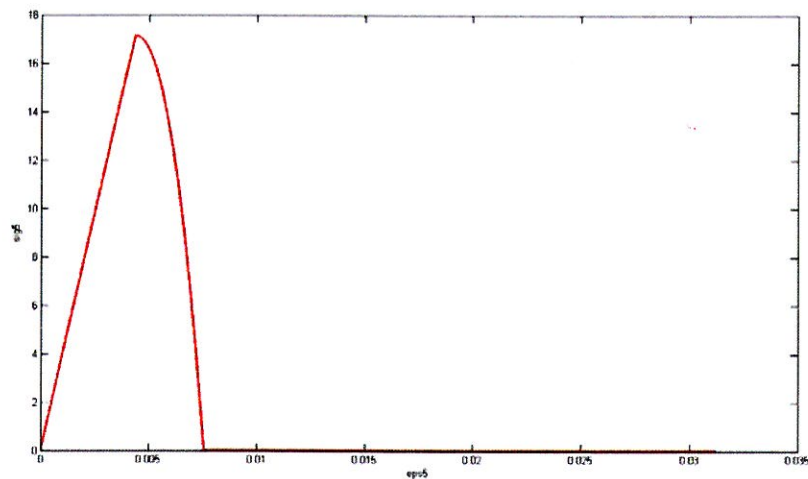
(Figure 4.17 – Stress strain curve for the cube in 1-3 plane)

4.13. Shear Stress-Strain relationship in 23 Plane

The analysis is set up such that there is positive shear in the 23 plane i.e., a positive transverse out of plane shear is defined for the composite laminate.

4.13.1. Results for the transverse out of plane shear test

The figure (4.18) shows the variation of in-plane stress with in-plane strain in the 23 plane.



(Figure 4.18 – Stress strain curve in the 2-3 plane)

4.14. Modes of damage observed in the single element tests

- **Fiber rupture**

From the figure (4.4), it can be observed that the damage initiation begins at approximately at a stress of 1950 MPa (Tensile Yield strength of the composite laminate along the fiber direction) and then on as damage accumulates; there is a gradual reduction in the stiffness of the composite laminate. There is a complete of stiffness at a strain of approximately 0.0225. Hence the model is able to capture the strain of “0.0075”, before complete failure.

From the figure (4.5), it can be seen that the damage growth function for fiber rupture is increasing monotonically over time. This goes to show that fiber rupture is well detected by the model.

- **Fiber buckling**

For the compression test it can be observed from the figure (4.6), it can be observed that the damage initiates at the -1950 MPa (Compressive Yield strength of the composite laminate along the fiber direction). Generally, the behavior of the composite in compression is different from its behavior in tension. But in the present case, since the compressive yield strength is assumed to be equal to its tensile yield strength, the damage initiation happens at the same stress level.

From the figure (4.7), it can be seen that the damage growth function for the fiber buckling is increasing monotonically over time. This goes to show that fiber buckling is well detected by the model.

- **Matrix cracking**

From the figures (4.8) and (4.12), it can be observed that stress strain curve has the same shape as that for tension tests in the fiber direction except that the damage initiation happens at a stress level of 48 MPa (Tensile yield strength in first transverse and second transverse direction). This behavior is observed as the yield strength in the first transverse direction is assumed to equal to the strength in the second transverse direction. This is so; because the composite laminate is assumed to be transversely isotropic in nature.

From the figures (4.9) and (4.13), it can be observed that the damage growth function for the matrix cracking in the first and second transverse direction increases monotonically over time and some oscillations can be observed towards the end of the simulation. The oscillations can be due to the explicit solver used.

- **Matrix crushing**

From the figures (4.10) and (4.14), it can be observed that stress strain curve has the same shape as that for tension tests in the fiber direction except that the damage initiation happens at a stress level of 48 MPa (Tensile yield strength in first transverse and second transverse direction). This behavior is observed as the yield strength in the first transverse direction is assumed to equal to the strength in the second transverse direction. This is so; because the composite laminate is assumed to be transversely isotropic in nature.

From the figures (4.11) and (4.15), it can be observed that the damage growth function for the matrix cracking in the first and second transverse direction increases monotonically over time and some oscillations can be observed towards the end of the simulation. The oscillations can be due to the explicit solver used.

- **Shear test**

From the figures for the shear stress strain curves in the 12 and 23 planes figure (4.16) and figure (4.18), it can be observed that the damage initiation (for the in plane shear, it initiates at 79 MPa, which is the in plane shear strength) and its progression is predicted well by the model.

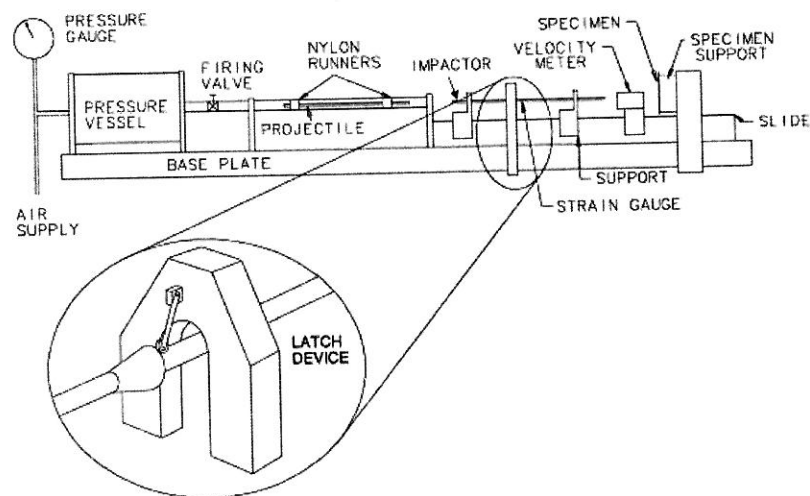
But from the figure (4.17) for the shear stress strain curve in the 13 plane, it can be observed that, there is no damage initiation predicted. Hence, the stress strain relation is linear and then there is damage accumulation.

4.15. Low-velocity impact analysis on composite target

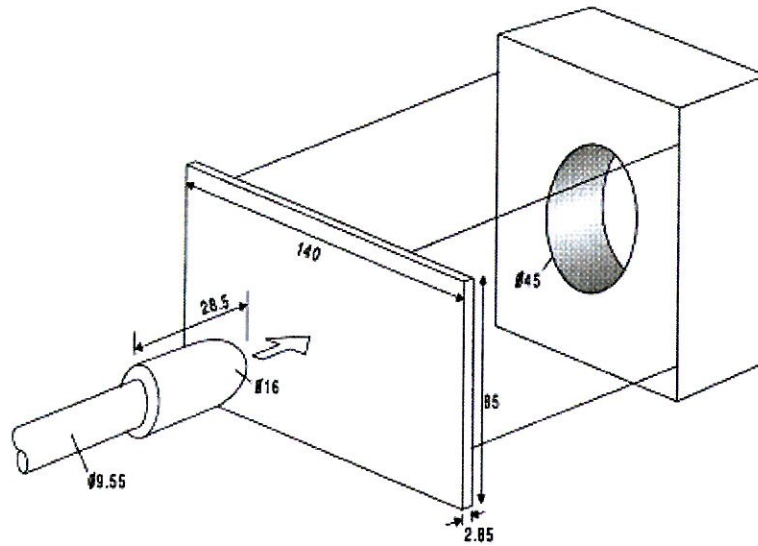
As the results for the single element tests are satisfactory, it can be concluded that the model is capable of capturing the various damage modes in the lamina. The model is capable of capturing fiber rupture, fiber kinking, matrix cracking and matrix crushing. With the confidence gained by the single element tests, the model is now used in a more complicated analysis that involves a low velocity impact on a composite target. This is done in order to further assess the capability of the model.

4.15.1. Experimental test and results

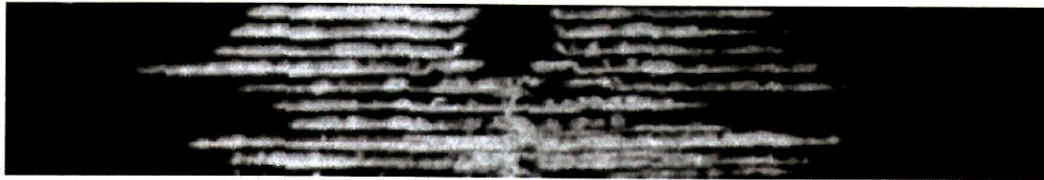
An experiment was conducted in [33]. It involved a low velocity impact on a target made of composite laminates by a titanium alloy impactor. The experimental setup is as shown in figure (4.19). The dimensions of the plate are 140 x 85 x 2.6 mm³. It is made up of unidirectional CFRP T300/914 laminates. The fiber volume fraction of the ply is 60%. The composite target plate has layup sequence of [0°] and [90°] alternate. The outermost plies are along the [0°] i.e., the longer side of the plate. The impactor has a mass of 260 g. The plate is supported by a support block, with a hole in center. The impactor impacts upon the target with a velocity of 7.080 m/s. More details regarding the test setup are available in [33].



(Figure 4.19 – Experimental setup for low-velocity impact test. After [32])



(Figure 4.20 – Experimental setup for target and the support. After [32])

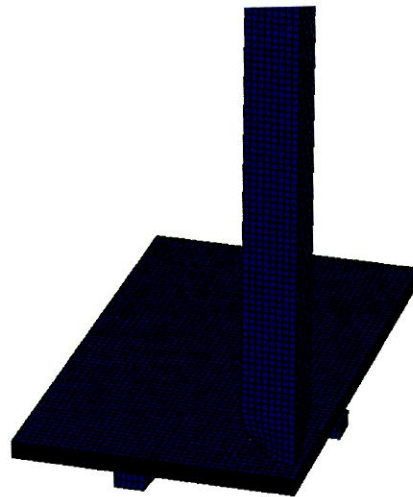


(Figure 4.21 – Delamination pattern observed in the target plate with a dye penetrant test. After [32])

The figure (4.20) shows the impactor and the target supported by the support block in detail. After the impact, the damage is detected using c-scan and dye penetrant. The figure (4.21) shows the delamination pattern when a section is taken in the center target along the short axis, after the impact.

4.15.2. Numerical simulation using the mixed mode damage model

The above low velocity impact test is simulated in Abaqus. The simulation is carried out with the composite target being modeled with the mixed mode damage model proposed by J.L. Curiel Sosa et al. [1]. The simulation involves a projectile impacting on to a target plate (made of composite laminates), supported by a circular ring. The target plate has 21 plies (0° and 90° alternate), with the outermost plies being along the 0° . The impactor is modeled as a cylinder (0.3 m long and 16 mm in diameter) with a hemispherical tip. It is made of titanium alloy, as this gives the same mass of 260 g (as applied in the tests). The support is modeled as a steel ring of 45 mm diameter. Due to symmetry reasons, the assembly is reduced to one-fourth of its total assembly. The assembly is set up as shown in the figure (4.19). The material properties for the steel and titanium alloy are specified as in table 4.2. Isotropic-elastic material models are used for both the support and the impactor.



(Figure 4.22 – Meshed geometry of the low velocity impact analysis)

MATERIAL	DENSITY (Ton/mm ³)	YOUNG'S MODULUS (MPa)	POISSON'S RATIO
Titanium Alloy	4.5E-009	116000	0.34
Steel	7.85E-009	210000	0.27

(Table 4.2- Table listing the properties specified for the impactor and the support)

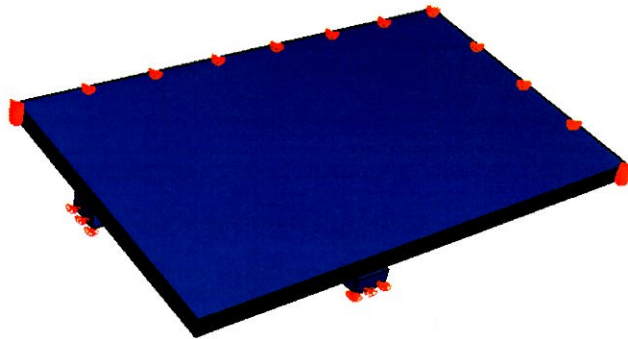
The material properties for the each of the plies in the target are specified as below in table 4.2.

PROPERTY	VALUE	UNITS
Density	1.58e-9	Ton/mm ³
E1(Young's Modulus along the fiber direction)	139000	MPa
E2(Young's Modulus along the first transverse direction)	9400	MPa
E3(Young's Modulus along the second transverse direction)	9400	MPa
G12(Shear Modulus in 1-2 direction)	4500	MPa
G23(Shear Modulus in 2-3 direction)	2980	MPa
G31(Shear Modulus in 3-1 direction)	4500	MPa
X11(Tensile Strength along the fiber direction)	2070	MPa
X22(Tensile Strength along the first transverse direction)	74	MPa
X33(Tensile Strength along the second transverse direction)	94	MPa
S12(Shear Strength in the 1-2 plane)	120	MPa
S23(Shear Strength in the 2-3 plane)	86	MPa
S31(Shear Strength in the 3-1 plane)	86	MPa
NU12 (Poisson's ratio)	0.0209	-
NU21(Poisson's ratio)	0.00141338	-
NU23(Poisson's ratio)	0.33	-
NU32(Poisson's ratio)	0.33	-
NU31(Poisson's ratio)	0.00141338	-
NU13(Poisson's ratio)	0.0209	-

(Table 4.3- Table listing the properties specified for the composite laminate)

A dynamic explicit step, with total time of "0.00042372 s" is defined. "Surface to surface" contact is defined between the surfaces of the support and the target and also between the surfaces of the impactor and the target. The boundary conditions on the target and the support are

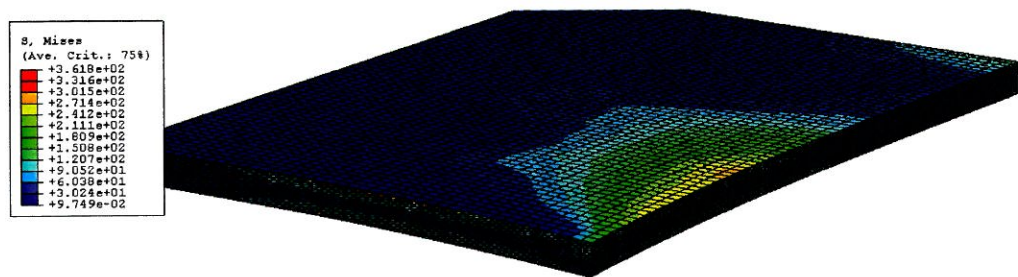
specified as shown in the figure (4.23), the edges of the target are fixed (in all the three directions) and so is the bottom surface of the support.



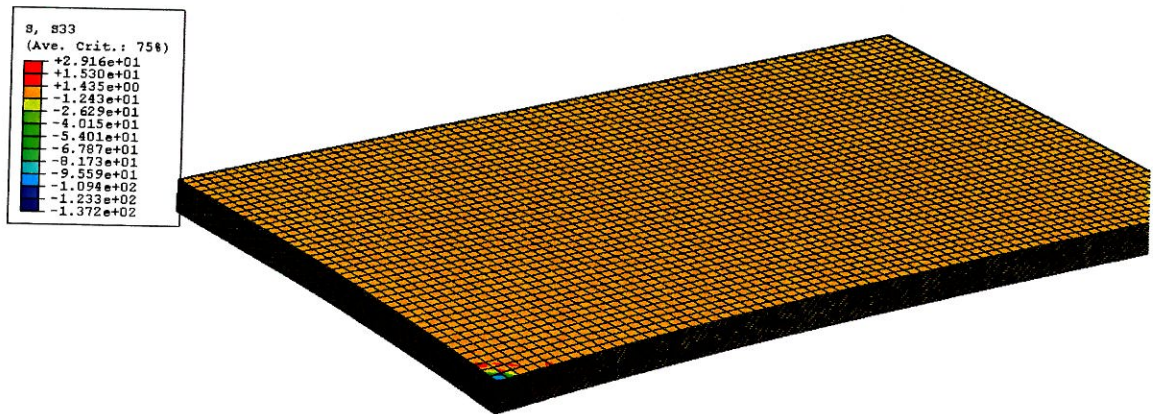
(Figure 4.23 – Boundary conditions specified on the target)

The target, impactor and the support are meshed with reduced integration hexagonal elements as shown in the figure (4.22).

The von-mises stress distribution in the target is as shown in the figure (4.24).



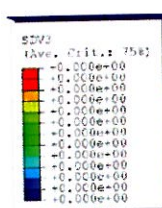
(Figure 4.24 – Von mises stress distribution on the target)



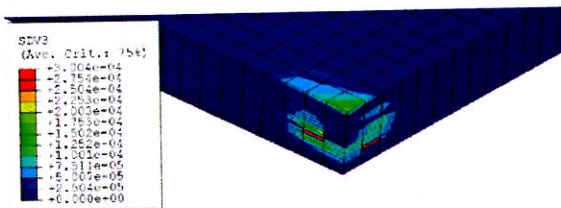
(Figure 4.25 – Distribution of stress component S33 on the target)

The distribution of component of stress “S33” i.e., stress in the normal direction over the target is as shown in the figure (4.25). The figure (4.26) shows the damage in the elements in the normal direction with increasing time. The state variable accumulating damage in the direction normal to the ply (mainly matrix cracking and matrix crushing) is plotted with progressing time. At “time = 0 s”, the impactor is not in contact with the target. At “time = 0.286 ms”, the contact between the impactor and the target has been established and hence there is damage in some of the elements. As time proceeds, there is growing contact between the target and the impactor and hence more elements of target are damaged and the damage within the elements also increases. At “time = 0.4237 ms”, the damage pattern in the elements at the end of the simulation, is as shown in the figure (4.26).

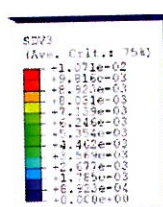
Time = 0 s



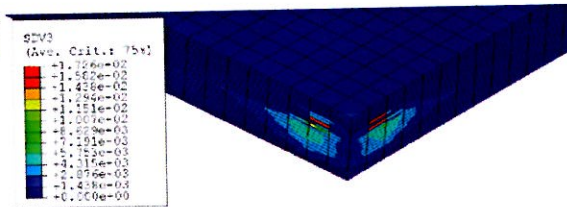
Time = 0.286 ms



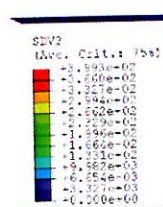
Time = 0.3072 ms



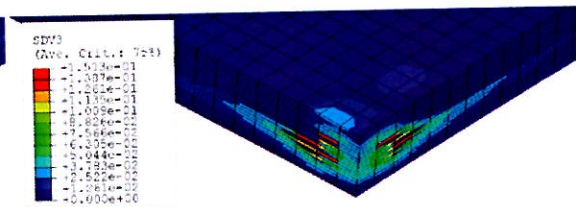
Time = 0.3389 ms



Time = 0.3813 ms



Time = 0.4237 ms



(Figure 4.26 - Damage in the normal direction)

4.15.3. Discussion of the results

From the figure (4.24), that shows the distribution of von mises stresses in the target, it can be noted that, the stresses are developed in the region close to the fixed edges and also near the support. The figure (4.25) shows the distribution of the S33 component of the stress in the target i.e., the component of stress in the direction normal to the plies. As a result of impact, these stresses are compressive in nature and result in the matrix crushing in the plies. Matrix crushing and cracking in the normal direction cause delamination in the laminate. Figure (4.26) shows in stages, the progressive growth of damage in the normal direction to the plies. The damage state

variable plotted in the figure accumulates damage in the normal direction and progressively degrades the stiffness properties in the direction normal to the plies. On the other hand, as expected, there is no fiber rupture or fiber kinking observed. The other important observation that can be made from the figure (4.25) is the symmetric nature of the damage about the corner of the target.

The damage pattern at “time = 0.4237 ms” resembles the damage pattern in the target in figure (4.21), obtained from the experimental results. As delamination is not explicitly considered in the implemented damage model, it cannot be predicted explicitly as a mode of damage. But, since matrix crushing and matrix cracking i.e., damage in the direction normal to the plies is the cause of delamination, it can be asserted confidently that, if the interfaces between elements damaged due to matrix crushing are modeled with cohesive elements, delamination can be observed clearly with the opening up of the interfaces.

This simulation result proves the capability of the model to predict the different damage modes i.e., matrix cracking, matrix crushing, fiber rupture and fiber kinking in accordance with the expectations, even in a complicated setup. The above simulation result also proves the ability of the model to work well with multiple elements.

5. Conclusions and Further Work

5.1. Conclusions

The use of composite materials in the industries, especially in the aircraft industry, has been increasing tremendously in the past years. This is due to the advantages such high strength to weight and high stiffness to weight ratios, it provides. So, as the usage increases, it becomes important to study the serviceability of composite aircraft structures. In order to predict the serviceability of composite structures, it becomes important to study the damage phenomenon when subjected to various loads. The aircraft structures are not only subjected to normal service loads, but also subjected to various hazards in mid air. The impact on air craft structures (such as wing, fan blade and windshield) due bird strike events being one the most common hazards in mid air. As, this event occurs in mid air and can cause serious problems, there is an impetus in the aircraft industries to study the failure behavior of composite structures subjected to high velocity impacts.

The failure behavior of aircraft composite structures can be studied by conducting with experimental tests (i.e., destructive testing). This approach has the disadvantage of high cost for the experimental test and also the loss of the specimen, as it will be complete unusable at the end of test.

The other approach is the computational simulation, where the experimental setup is mimicked in the computer environment. For this approach to predict the failure of composite structures successfully, it becomes important that the loads on the specimen geometry along with boundary conditions are specified very accurately. Apart from this, the behavior of the composite structure should be represented with appropriate models, which exactly describe the constitutive relationship.

In the past years, lot of research work has been done in this area to define appropriate constitutive relationships for composite structures that represent their behavior exactly. There are various failure theories and models developed. Some of the failure theories are mere extension of the failure theories for ductile materials. There are models developed which consider the non-linear stress strain relationship after failure initiation, but most of them are limited to applications with two dimensional elements.

In this thesis, work is done to evaluate the state of art failure theories. These theories seem to predict a damage pattern in the composite laminates that does not match exactly with the experimental results. The evaluation of the theories is done with the help of a progressive failure methodology.

The main focus of the thesis is the implementation of the three dimensional mixed mode model for composite material structures. The implementation has been done in the Abaqus subroutine VUMAT. The Abaqus explicit solver is used for solving the dynamic equilibrium equation. The explicit time integration scheme used by the Abaqus solver is the well known "explicit central difference method". The choice of explicit solver is made by keeping in mind the advantages of the explicit solver when considering large models such as impact are considered.

The tension, compression and shear tests have been conducted for a single element. The strain-stress curves closely matches with the experimental result and depicts the gradual decrease of the stiffness after failure initiation. Most importantly, the model has been able to capture the small amount of strain the specimen can withstand before complete failure. It is also found to detect different damage modes at the right state of stress. The satisfactory results for the tension and compression tests along three perpendicular directions confirm the three dimensional nature of the model.

A low velocity impact simulation has been conducted to further assess the capability of the model in predicting damage in a more complicated, multi element setup. The model successfully predicts damage in the direction normal to the plies. The damage in the direction normal to the plies is mainly responsible for causing delamination in the laminate and hence in a way the model is capable of predicting delamination. The damage pattern obtained as a result of the simulation closely matches with the experimental results.

5.2. Future Work

- As delamination as a damage mode is not explicitly considered in the model, only the delamination areas are predicted by the model. Going further, a formulation including the delamination explicitly could be investigated.
- A further research could be done in order to include the non-linear elastic stress strain behavior of composite materials when subjected to shear.
- The shear stress-strain behavior in the 13 plane has to be modified in order to fit better with the experimental results.
- In a high velocity impact situation the elements are undergoing excessive distortion. This is due to the fact that the explicit time integration scheme becomes unstable after a while.
- Modifications of the damage surfaces could enhance the model.
- Calibration of the directional damage vectors could also enhance the model

References

- [1] Curiel Sosa J.L., Petrinic N. and Wiegand J. A three-dimensional progressive damage model for fibre-composite materials. *Mechanics Research Communications*, 35 (2008), 219-221.
- [2] Hinton M.J. and Soden P.D. Predicting failure in composite laminates: the background to the exercise. *Compos. Sci. Technol.*, 58 (1998), 1001-1010.
- [3] Hinton M.J., Kaddour A.S. and Soden P.D. A further assessment of the predictive capabilities of current failure theories for composite laminates: Comparison with experimental evidence. *Compos Sci. Technol.*, 64 (2004), 549-588.
- [4] Soden P.D., Hinton M.J. and Kaddour A.S. A comparison of the predictive capabilities of current failure theories for composite laminates. *Compos. Sci. Technol.*, 58 (1998), 1225-1254.
- [5] Soden P.D., Hinton M.J. and Kaddour A.S. Lamina properties, lay-up configurations and loading conditions for a range of fibre-reinforced composite laminates. *Compos. Sci. Technol.*, 58 (1998), 1011-1022.
- [6] Daniel IM. Failure of composite materials. *Strain*, 43, 4-12, 2007.
- [7] Cuntze R.G. and Freund A. The predictive capability of failure mode concept-based strength criteria for multidirectional laminates. *Compos. Sci. Technol.*, 64 (2004), 343-377.
- [8] Tan S.C. A progressive failure model for composite laminates containing openings. *J. Composite Mater.* 25 (1991), 556-577.
- [9] Harris C.E., Coats T.W., Allen D.H. and Lo D.C. A progressive damage model and analysis methodology for predicting the residual strength of composite laminates. *J. Compos. Technol. Res.*, 29 (1995), 926-981.
- [10] Hochard C., Auburg P.A. and Charles J.P. Modelling of the mechanical behaviour of woven fabric CFRP laminates up to failure. *Compos. Sci. Technol.*, 61(2001), 221-230.
- [11] Edlund U. and Volgers P. A composite ply failure model based on continuum damage mechanics. *Composite Structures*, 65 (2004), 347.

- [12] Talreja R. Modelling of damage development in composites using internal variables concepts. Proceedings of the ASME, Damage Mechanics in Composites, AD, 12 (1987), 11-16.
- [13] Allen D.H., Harris C. and Groves S.E. A thermomechanical constitutive theory for elastic composites with distributed damage. Part I: theoretical development. Int. J. Solids Struct. 23 (1987), 1301-1318.
- [14] Chang F-K. and Chang K.Y. A progressive damage model for laminated composites containing stress concentration. J. Composite Mater., 21 (1987), 834-855.
- [15] Shahid I. and Chang F-K. An accumulative damage model for tensile and shear failure of laminated composite plate. J Compos Mater, 29 (1995), 926-981.
- [16] Lessard L.B. and Shokrieh M.M. 2-D modelling of composite pinned-joint failure. J. Composite Mater. 29 (1995), 671-697.
- [17] Camanho P.P. and Mathews F.L. A progressive damage model for mechanically fastened joints in composite laminates. J. Composite Mater. 33 (1999), 2248-2280.
- [18] Camanho P.P., Dávila C.G. and de Moura M.F. Numerical simulation of mixed-modes progressive delamination in composite materials. J. Composite Mater. 37 (2003), 1415-1438.
- [19] Zohdi T., Feucht M., Gross D. and Wriggers P. A description of macroscopic damage through microstructural relaxation. Int. J. Numer. Meth. Engn. 43 (1998), 493-506.
- [20] Robert.M.Jones, Mechanics of Composite materials.
- [21] A. Puck & H. Schürmann. Failure analysis of FRP laminates by means of Physically based phenomenological models. Composites Science and Technology 58 (1998) 1045±1067.
- [22] A. Matzenmiller, J. Lubliner and R.L.Taylor. A constitutive model for anisotropic damage in fiber composites. Mechanics of Materials 20 (1995) 125-152.
- [23] P.Maimi, J.A. Mayugo and P.P. Camanho. A three-dimensional damage model for transversely isotropic composite laminates. Journal of composite materials 42 (2008) 2717-2745.
- [24] Mohit Garg, Galib H. Abumeri and Dade Huang. Predicting Failure Design Envelop for Composite Material System Using Finite Element and Progressive Failure Analysis Approach. SAMPE 2008 Conference paper.

- [25] D. Huang, Frank Abdi and Ayman Mosallam. Comparison of failure mechanism in composite structure. SAMPE 2003 Conference paper.
- [26] GENOA User Manual. <http://www.ascgenoa.com>.
- [27] Chaboche J-L. Continuous Damage Mechanics—a tool to describe phenomena before crack initiation. Nucl. Engng. Des., 64 (1998), 233-247.
- [28] Lemaitre J. and Chaboche J-L. Mechanics of Solids Materials. Cambridge. (University Press, 1990).
- [29] J.L. Curiel Sosa. A Novel Directional Damage Model for Composites. Proceedings of the Ninth International Conference on Computational Structures Technology.
- [30] Curiel Sosa J.L., de Souza Neto E. and Owen D.R.J. A combined implicit-explicit algorithm in time for non-linear finite element analysis. Commun. Numer. Meth. Engng., 22 (2006), 63-75.
- [31] Abaqus Documentation.
- [32] J.P. Hou, N. Petrinic, C. Ruiz, S.R. Hallett. Prediction of impact damage in composite plates. Composites Science and Technology 60 (2000) 273±281.
- [33] J.P. Hou, N. Petrinic, C. Ruiz. A delamination criterion for laminated composites under low-velocity impact. Composites Science and Technology 61 (2001) 2069–2074.

Errata and clarifications

Three dimensional modelling of fibre reinforced composite materials for aerospace applications

Shankara Narayana Phaneendra

Corrections

Page	Reads	Should read
Page No 30, equation (4.6)	$B(\omega) = \begin{bmatrix} (1 - \omega_{11})G_{12} & 0 & 0 \\ 0 & (1 - \omega_{11})G_{23} & 0 \\ 0 & 0 & (1 - \omega_{11})G_{31} \end{bmatrix}$	$B(\omega) = \begin{bmatrix} (1 - \omega_{12})G_{12} & 0 & 0 \\ 0 & (1 - \omega_{23})G_{23} & 0 \\ 0 & 0 & (1 - \omega_{13})G \end{bmatrix}$
Page No 32, equation (4.16)	$F_{11}^{N+1} = \frac{\sigma_{11}^2}{(1 - \omega_{11})^2 \cdot X_{11}^2} + \frac{\sigma_{12}^2}{(1 - \omega_{12})^2 \cdot X_{12}^2} + \frac{\sigma_{13}^2}{(1 - \omega_{13})^2 \cdot X_{13}^2}$	$f_{11}^{N+1} = \frac{\sigma_{11}^2}{(1 - \omega_{11})^2 \cdot X_{11}^2} + \frac{\sigma_{12}^2}{(1 - \omega_{12})^2 \cdot X_{12}^2} + \frac{\sigma_{13}^2}{(1 - \omega_{13})^2 \cdot X_{13}^2}$
Page No 32, equation (4.17)	$F_{11}^{N+1} = \frac{\sigma_{22}^2}{(1 - \omega_{22})^2 \cdot X_{22}^2} + \frac{\sigma_{12}^2}{(1 - \omega_{12})^2 \cdot X_{12}^2} + \frac{\sigma_{13}^2}{(1 - \omega_{13})^2 \cdot X_{13}^2}$	$f_{11}^{N+1} = \frac{\sigma_{22}^2}{(1 - \omega_{22})^2 \cdot X_{22}^2} + \frac{\sigma_{12}^2}{(1 - \omega_{12})^2 \cdot X_{12}^2} + \frac{\sigma_{13}^2}{(1 - \omega_{13})^2 \cdot X_{13}^2}$
Page No 32, equation (4.18)	$F_{11}^{N+1} = \frac{\sigma_{33}^2}{(1 - \omega_{33})^2 \cdot X_{33}^2} + \frac{\sigma_{31}^2}{(1 - \omega_{31})^2 \cdot X_{31}^2} + \frac{\sigma_{32}^2}{(1 - \omega_{32})^2 \cdot X_{32}^2}$	$f_{11}^{N+1} = \frac{\sigma_{33}^2}{(1 - \omega_{33})^2 \cdot X_{33}^2} + \frac{\sigma_{31}^2}{(1 - \omega_{31})^2 \cdot X_{31}^2} + \frac{\sigma_{32}^2}{(1 - \omega_{32})^2 \cdot X_{32}^2}$
Page No 33, equation (4.23)	$\omega^{N+1} = \dot{\omega}^{N+1} \cdot \Delta t$	$\Delta \omega^{N+1} = \dot{\omega}^{N+1} \cdot \Delta t$
Page No 33, equation (4.24)	$\omega = \omega + \Delta \omega^{N+1}$	$\omega^{N+1} = \omega^N + \Delta \omega^{N+1}$

Clarifications

- The unit of stress measure in the figures (4.4), (4.6), (4.8), (4.10), (4.12), (4.14), (4.16), (4.17) and (4.18) is MPa.
- The unit of time measure in the figures (4.5), (4.7), (4.9), (4.11), (4.13) and (4.15) is seconds.